Stress in western Canada from regional moment tensor analysis[1]

John Ristau, Garry C. Rogers, and John F. Cassidy

Abstract: More than 180 regional moment tensor (RMT) solutions for moderate-sized earthquakes (M ≥ 4) are used to examine the contemporary stress regime of western Canada and provide valuable information relating to earthquake hazard analysis. The overall regional stress pattern shows mainly NE–SW-oriented *P* axes for most of western Canada with local variations. In the northern cordillera, the maximum compressive stress direction (σ1) varies from east–west to north–south to NE–SW from south to north. The stress direction σ1 is consistent with the *P* axis direction for the largest earthquakes, except in the central and northern Mackenzie Mountains where there is a 16° difference. The Yakutat collision zone shows a steady change in σ1 from east–west in the east to north–south in the west. In the Canada – United States border region, RMT solutions suggest a north–south compressional regime may extend through southern British Columbia and northern Washington to the eastern Cordillera. In the Vancouver Island – Puget Sound region, RMT solutions do not show any obvious pattern in faulting style. However, the stress results are consistent with margin-parallel compression in the crust and downdip tension in the subducting slab. Along the Queen Charlotte fault σ1 is oriented ~45° to the strike of the northern section of the fault, which is dominated by strike-slip faulting, and ~60° to the strike of the southern section, which is dominated by high-angle thrust faults. The amount of thrust faulting infers a significant amount of convergence between the Pacific and North America plates in the southern Queen Charlotte Islands region.

Résumé : Plus de 180 solutions régionales de tenseur de moment, pour des séismes de taille modérée (M ≥ 4) sont utilisées pour examiner le régime des contraintes contemporaines dans l'Ouest canadien et fournir des informations utiles concernant l'analyse des risques sismiques. Le patron global des contraintes régionales montre une orientation principale NE–SO de l'axe *P* pour la plus grande partie de l'Ouest canadien, avec quelques variations locales. Dans la cordillère septentrionale, la principale direction de contrainte de compression (σ1) varie de E–O, à N–S, à NE–SO du sud vers le nord. La contrainte σ1 concorde avec la direction de l'axe *P* pour les plus grands séismes sauf pour les monts Mackenzie centre et nord, où il existe une différence de 16°. La zone de collision de Yakutat montre que σ1 change progressivement de E–O à l'est à N–S à l'ouest. Dans la région de la frontière Canada – États-Unis, les solutions régionales de tenseur de moment suggèrent un régime possible de compression N–S qui s'étendrait à travers le sud de la Colombie-Britannique et le nord de l'état de Washington vers la cordillère orientale. Dans la région de l'île de Vancouver – Puget Sound, les solutions régionales de tenseur de moment ne présentent aucun patron évident de style de failles. Toutefois, les résultats des contraintes concordent avec une compression parallèle à la bordure dans la croûte et une tension selon le pendage dans la dalle de subduction. Le long de la faille de la Reine-Charlotte, σ1 a une orientation de ~45° par rapport à la direction de la section nord de la faille, laquelle est dominée par des failles de décrochement, et de ~60° par rapport à la section sud, laquelle est dominée par des failles de chevauchement à pendage abrupt. La quantité de failles de chevauchement signifie une grande convergence entre les plaques pacifique et nord-américaine dans la région sud des îles de la Reine-Charlotte.

[Traduit par la Rédaction]

Introduction

The purpose of this study is to examine the contemporary seismotectonic setting of western Canada using earthquake focal mechanisms, which offer one of the best methods to study active tectonics. We use broadband data from the recently established three-component seismograph network in western Canada, the Pacific Northwest of the United States, and eastern Alaska to calculate regional moment tensor (RMT) solutions for moderate-sized earthquakes (M ≥ ~4) in

Received 20 June 2005. Accepted 25 May 2006. Published on the NRC Research Press Web site at http://cjes.nrc.ca on 23 March 2007.

Paper handled by Associate Editor F. Cook.

J. Ristau,[2,3] G.C. Rogers, J.F. Cassidy. School of Earth and Ocean Sciences, University of Victoria, Victoria, BC V8L 3P6, Canada; Geological Survey of Canada, Pacific Geoscience Centre, P.O. Box 6000, Sidney, BC V8L 4B2, Canada.

[1]Gelogical Survey of Canada, Contribution 20060666.
[2]Corresponding author (e-mail: jristau@nrcan.gc.ca).
[3]Current address: GNS Science, P.O.Box 30368, Lower Hutt, New Zealand.

 doi:10.1139/E06-057

western Canada. The source parameters (strike, dip, slip, seismic moment) and depths derived from the RMT solutions are then used to investigate the current stress regime in the Canadian Cordillera, the Vancouver Island – Puget Sound region, and the Queen Charlotte Islands region.

Western Canada is a large and tectonically diverse region and encompasses some of the most, and least, seismically active areas in Canada. Western Canada is defined here as the region seaward of the Foreland Fold and Thrust Belt, extending from the Canada – United States border in the south through to the Beaufort Sea in the north, and including the Queen Charlotte Islands and Vancouver Island – Puget Sound regions (Fig. 1). The main influences on the tectonics of western Canada are the relative motion of the Pacific and North America plates along the west coast of North America and the subduction of the Juan de Fuca plate beneath North America.

The Cascadia subduction zone is a high-seismicity region of active plate convergence where the Juan de Fuca plate, a small oceanic plate between the North America and Pacific plates, is subducting beneath North America (Fig. 2). The Cascadia subduction zone also includes two smaller plates that act independently of the Juan de Fuca plate — the Explorer plate to the north and the Gorda plate to the south (see Riddihough 1977; Menard 1978; Riddihough 1984; Wilson 1988; Atwater 1989 for details). The seismic activity in the Vancouver Island – Puget sound region is concentrated along the west coast of Vancouver Island and around southeast Vancouver Island and northwest Washington. No megathrust earthquakes have been detected on the Juan de Fuca subduction interface in historical times (the last ~200 years) although the subduction zone is currently locked and accumulating strain toward a future megathrust earthquake (e.g., Dragert et al. 1994; Hyndman and Wang 1995; Mazzotti et al. 2003*a*). Earthquakes occur in both the overlying North America continental crust (overlying crust events) and within the subducting Juan de Fuca plate (in-slab events) (e.g., Rogers 1998). North of the Cascadia subduction zone is the Queen Charlotte Islands margin with the dominant tectonic feature being the Queen Charlotte fault zone, which forms the boundary between the Pacific and North America plates (Fig. 1). Seismicity is associated with the Queen Charlotte fault and also occurs in the Queen Charlotte Islands region east of the Queen Charlotte fault (Fig. 2).

North of the Queen Charlotte Islands region is a region of high seismicity where the Yakutat block, a composite oceanic–continental allochthonous terrane that has migrated northward with the Pacific plate, is colliding with North America in the Gulf of Alaska (e.g., Lahr and Plafker 1980; Plafker et al. 1994). East of the Yakutat collision the seismicity decreases rapidly indicating little deformation in this region (Fig. 2). Seismicity increases significantly in the Richardson and Mackenzie Mountains region more than 600–800 km northeast of the plate boundary (Fig. 2). This is a region of numerous geologically mapped strike-slip and low-angle thrust faults, along which most of the seismicity likely occurs (see Hoffman and Bowring 1984; Hildebrand et al. 1987; Isachsen and Bowring 1994 for a history of the northern Cordillera). Mazzotti and Hyndman (2002) proposed that deformation in this region results from a transfer of strain from the Yakutat collision zone across the northern Cordillera. Large (M 6.0–6.5) events have occurred throughout this region in recent times (e.g., Wetmiller et al. 1988; Cassidy and Bent 1993; Cassidy et al. 2002). Cassidy et al. (2005) give a detailed overview of the current seismicity of the northern Canadian Cordillera. The southern Canadian Cordillera is a region of relatively low seismic activity compared with the northern Cordillera (Fig. 2). The rate of seismicity in the southern Cordillera quickly drops inland from the coast and increases to the east in the region of the Rocky Mountain trench and western Alberta, and to the south in the vicinity of the Canada – United States border. Monger and Price (1979) provide an overview of the tectonic evolution of the southern Cordillera.

Information on crustal stresses in Canada has increased substantially in the last 25 years. Adams (1987) began compiling information from a variety of sources including focal mechanisms, oil well breakouts, hydraulic fracturing, and overcoring (Adams and Bell 1991), and data are compiled in the Canadian Crustal Stress Database (CCSB). Very few focal mechanisms (~15) exist in the CCSB for the Yukon Territory – Northwest Territories and British Columbia regions. Stress information for the continental region of western Canada in the CCSB is mainly limited to oil well breakouts in western Alberta and in the Mackenzie delta region of the Northwest Territories (Adams 1987; Adams and Bell 1991). With the ability to calculate RMT solutions, there are now more than 170 moment tensor solutions available for the Canadian Cordillera, Queen Charlotte Islands, and Vancouver Island – Puget Sound regions. Many of these solutions are located where previous stress information is not available from oil well breakouts or any previously calculated focal mechanisms. As a result this is the first analysis of crustal stresses from focal mechanisms for much of western Canada and includes stress information at depth which was not available previously.

Methods

Regional moment tensor analysis

Moment tensor analysis involves fitting theoretical waveforms with observed broadband waveforms from earthquakes. The procedure gives the magnitude of the earthquake, fault orientation, type of motion on the fault, and depth, and can be used to determine the stress and strain fields.

Since the mid-1990s, more than 40 three-component broadband seismometers have been installed in western Canada, the Pacific Northwest of the United States, and eastern Alaska, now providing high-quality seismic data suitable for moment tensor analysis (Fig. 1). The broadband data, along with increased computing power, has made it possible to routinely calculate RMT solutions for smaller earthquakes ($M \geq \sim 4.0$) in western Canada and adjacent regions. RMT solutions differ from teleseismic moment tensor methods (e.g., Harvard centroid moment tensor (CMT) solutions and United States Geological Survey (USGS) moment tensor solutions) in that they use regional data (source–receiver distances of ~1000 km or less) and region-specific Earth models. Earthquakes with $M > \sim 5.0$–5.25 generate a significant amount of low-frequency energy (e.g., <0.025 Hz) and the waveforms at these low frequencies can be modelled using simple whole Earth models. Earthquakes with $M \leq \sim 5.0$ do not gen-

Fig. 1. Major tectonic features of western Canada and adjacent regions. Black dots are locations of three-component broadband seismometers in western Canada, Washington, and eastern Alaska used to calculate regional moment tensor solutions. The inset defines the various sub-regions for western Canada that are discussed in this study.

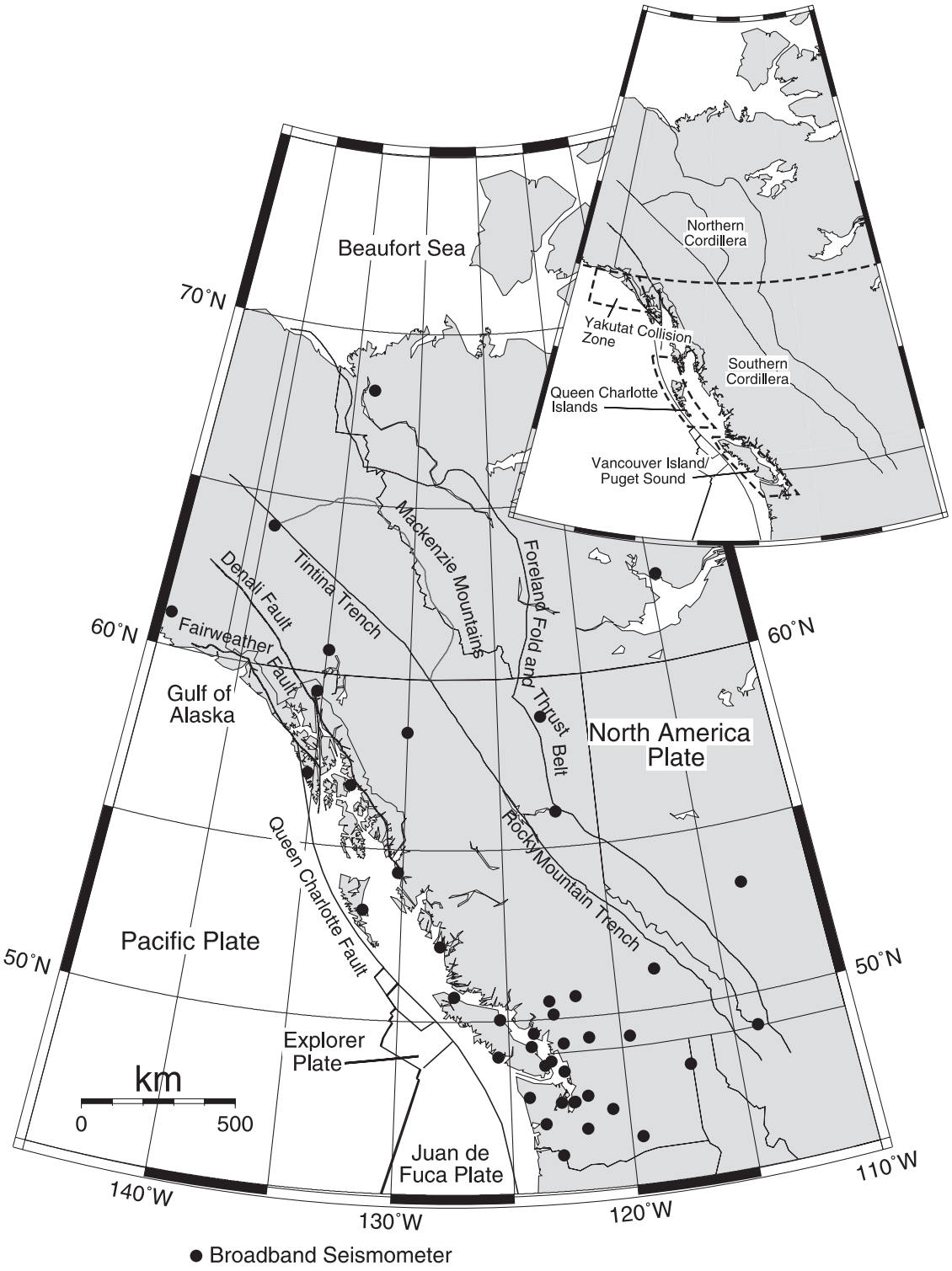

erate energy at low frequencies, and higher frequencies must be used for the moment tensor analysis. A generic whole Earth model is no longer sufficient, and Earth models specific to the source–receiver travel path must be used to accurately model the observed waveforms (see Ristau (2004) for details on the velocity models used). By extending the magnitude threshold down to M ~4.0, it has been possible to calculate ~10 times as many moment tensor solutions compared with teleseismic methods.

RMT solutions have been calculated on a routine basis at

Fig. 2. Seismicity (1984–2004) of the Canadian Cordillera and adjacent regions. The regions of high seismicity include the offshore region of British Columbia through to the Yakutat collision zone, the Vancouver Island – Puget Sound region, and the northern cordillera. Mag, magnitude.

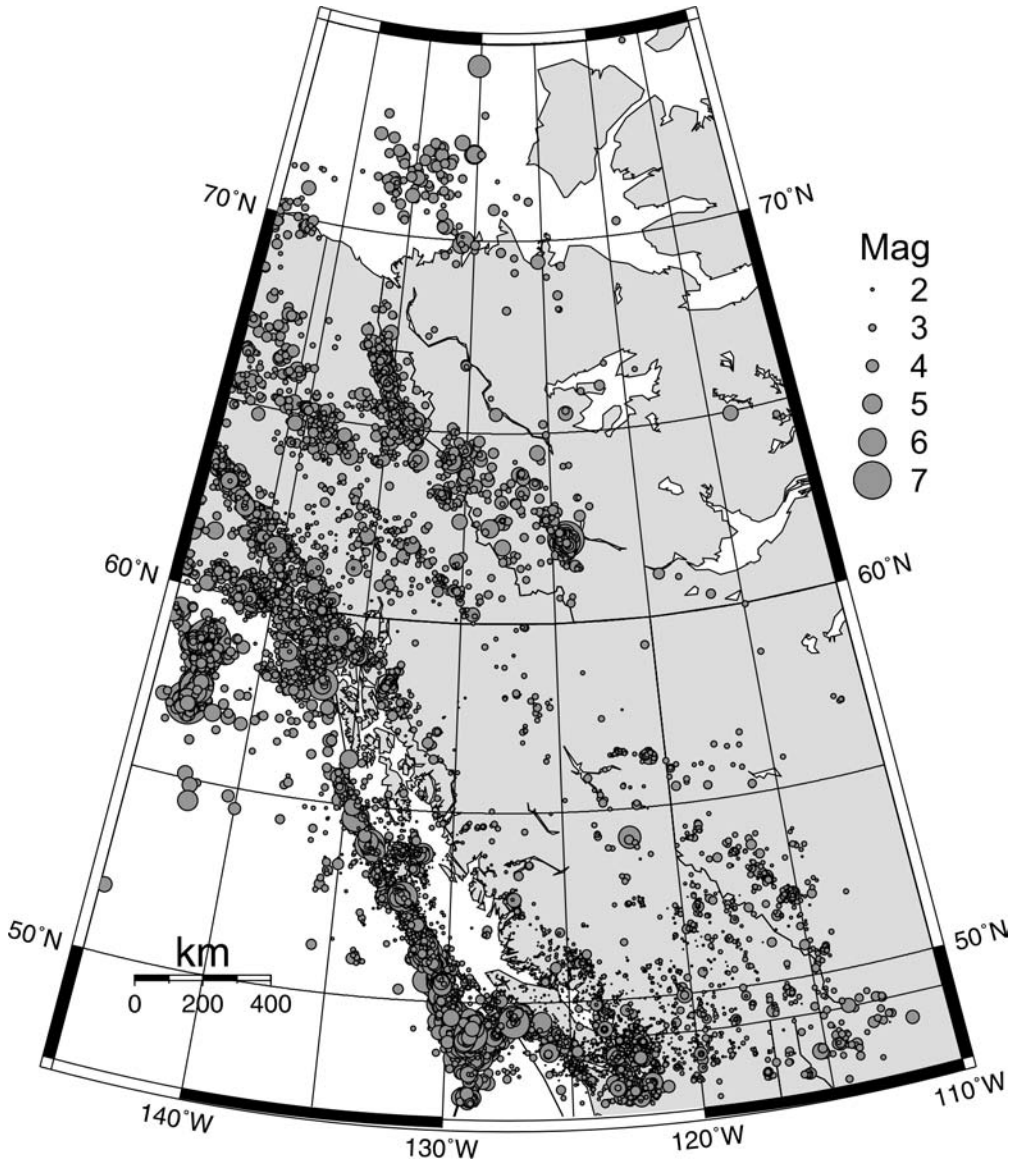

the Pacific Geoscience Centre (PGC) of the Geological Survey of Canada since 2001 (e.g., Ristau et al. 2003, 2005) using the code of Ammon (2001) as developed for use on smaller magnitude earthquakes. A catalogue now exists back to the beginning of 1995. Extensive details on the moment tensor algorithm can be found in Ammon (2001). In most cases, the observed waveforms are bandpass filtered between 20 and 50 s (0.02–0.05 Hz), with passbands frequencies as high as 12.5–25 s (0.04–0.08 Hz) being used for the smallest events. Harvard CMT solutions use waveform energy with periods >45 s (<0.022 Hz) (Dziewonski et al. 1981), and USGS solutions use a 15–55 s (0.018–0.067 Hz) passband (Sipkin 1986). The Green's functions are calculated using simple 1-dimensional Earth models appropriate to the source region and are filtered using the same bandpass range as the observed waveforms. Using the observed waveforms and the Green's functions, the moment tensor elements are found using a least squares time-domain moment tensor inversion scheme described by Langston (1981). Solutions are calculated over a range of depths, typically every 3 km, to find the depth that minimizes the misfit between the synthetic and observed waveforms. The RMT solutions have been compared with Harvard CMT solutions where available, and there is excellent agreement in both moment (M_o) and focal mechanisms.

To the end of 2004, more than 420 RMT solutions have been calculated for western Canada and adjacent regions with moment magnitudes (M_w) ranging from M_w = 3.4–6.8 (Fig. 3). In addition to the RMT solutions calculated in this study, Oregon State University (OSU) calculated RMT solutions for much of western Canada south of ~55°N from 1994 to 1998 (Braunmiller and Nábělek 2002). Most of the OSU RMT solutions have been recalculated in this study to have a consistent data set. The RMT solutions calculated in this study are very similar to the OSU solutions. Waveform

Fig. 3. Focal mechanisms calculated for western Canada and adjacent regions from 1976–2004. RMT solutions calculated in this study are in black; Oregon State University (OSU) RMT solutions calculated in 1994–1995, Harvard CMT solutions for 1976–1993, and first-motion solutions are in grey.

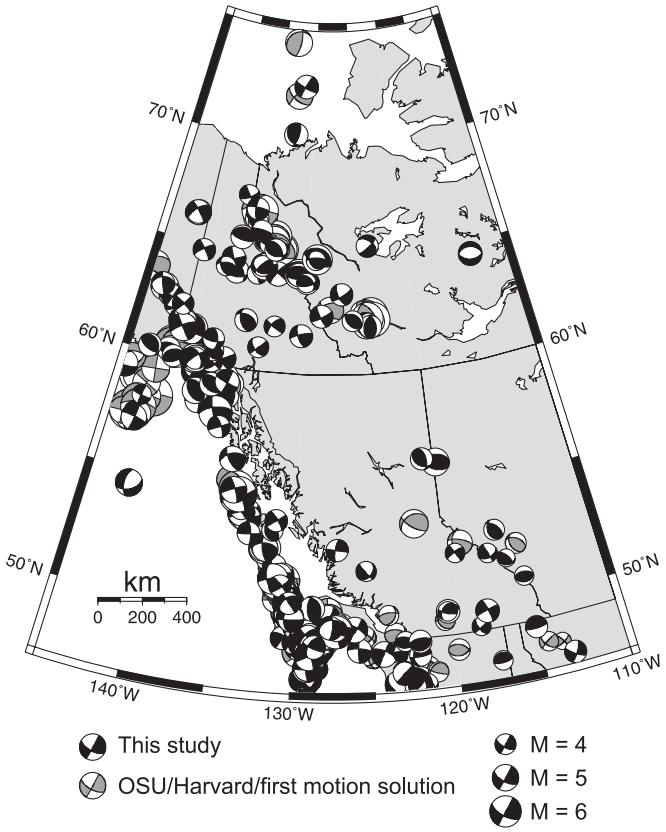

data were not available for 14 events in 1994 and 1995. Therefore, the OSU RMT solutions for those 14 events are included in the data set. For events earlier than 1994, only Harvard CMT solutions are available, and several first-motion focal mechanisms are also included in the data set.

Stress tensor analysis

Several inversion schemes have been developed for calculating composite stress tensors from earthquake focal mechanisms, including Michael (1984), Gephart and Forsyth (1984), and Angelier (1984). In this study, stress tensors are calculated with ZMAP6 (Wiemer 2001) using the method of Michael (1987), an extension of the Michael (1984) method. The Michael (1987) method does not require the fault plane to be chosen a priori.

To define the stress field of a region from focal mechanisms, a number of mechanisms must be available. McKenzie (1969) showed that the maximum compressive stress may have an orientation anywhere within the dilatational quadrant of the focal mechanism, and that the pressure (*P*) and tension (*T*) axes from a single fault plane solution may vary significantly from the principal stress directions depending on the orientation and strength of the faults. This means that the principal stresses are poorly constrained by a single focal mechanism or many mechanisms with similar orientations and slip directions. However, if there are a variety of focal mechanisms on faults with different orientations within a region of uniform stress then the principal stress directions can be determined. In the Michael (1987) method, the stress tensor is calculated using a linear least-squares inversion technique to find the stress model that most closely matches the observed data. The assumptions are that slip on the fault plane occurs in the direction of the resolved shear stress and that the stress orientation is homogenous in the selected volume.

Results

Overall crustal stress pattern in western Canada

The regional stress pattern from earthquake focal mechanisms can be mapped by plotting the principal stress directions. This is most effective when the principal axes are horizontal or near-horizontal. Virtually all focal mechanisms in western Canada are strike-slip or thrust. Therefore, the maximum compressive stress axes will be near-horizontal and the compressive stress direction can be represented by plotting the azimuth of the *P* axis (Fig. 4). To reflect the varying plunge of the *P* axis, the arrows are scaled according to the plunge, with a 0° plunge being the largest and 90° plunge having zero length. Also shown in Fig. 4 are stress directions from the world stress database taken mainly from oil well breakouts. As can be seen in Fig. 4, the stress information from the moment tensor solutions and from the world stress database for the most part do not overlap. Figure 5 plots the *T* axis azimuth for the same focal mechanisms as in Fig. 4. A plunge close to 0° in the *T* axis plot corresponds to strike-slip or normal faulting, and a plunge close to 90° corresponds to thrust faulting.

The overall compressive stress pattern is relatively straightforward for most of western Canada. In the northern Canadian Cordillera; the compressive stress is mainly oriented in a NE–SW direction from the Gulf of Alaska through to the Mackenzie Mountains. In the eastern Canadian Cordillera, around the British Columbia – Alberta border region, the compressive stress direction is NE–SW, consistent with Adams (1987), and supports the idea that the whole of the Canadian Cordillera is being compressed in a NE–SW direction.

The exception is in southwest British Columbia and northwest Washington where the compressive stress direction is north–south. One major factor in this stress regime is oblique subduction of the Juan de Fuca plate and right-lateral shear motion of the Pacific and North America plates, causing north–south compression (Wang et al. 1997). Wang et al. (1997) concluded that the most important roles in the stress regime of the Juan de Fuca plate are a compressional force normal to the Mendocino transform fault at the southern end of the plate, a result of the northward push by the Pacific plate, and a horizontal resistance operating against the northward, or margin-parallel, component of oblique subduction. In southwest British Columbia and northwest Washington, the Juan de Fuca plate is strongly coupled with the North America plate and results in margin-parallel compression in the continental crust. In the eastern Cordillera, the Juan de Fuca plate no longer influences the North America plate and compressive crustal stresses are similar with the rest of Canada. The other major factor is the breaking up of the Cascadia fore arc into large rotating blocks (Wells et al. 1998). Wells et al. (1998) identified three fore-arc blocks: the Washington

Fig. 4. *P* axis azimuths from focal mechanisms in western Canada along with compressive stress directions from the world stress database. The arrow lengths are scaled according to the plunge of the axis, with 0° plunge being the longest and 90° having zero length. The compressive stress direction is generally oriented NE–SW for most of western Canada, with the exception of southwest British Columbia and northwest Washington where the compressive stress direction is north–south.

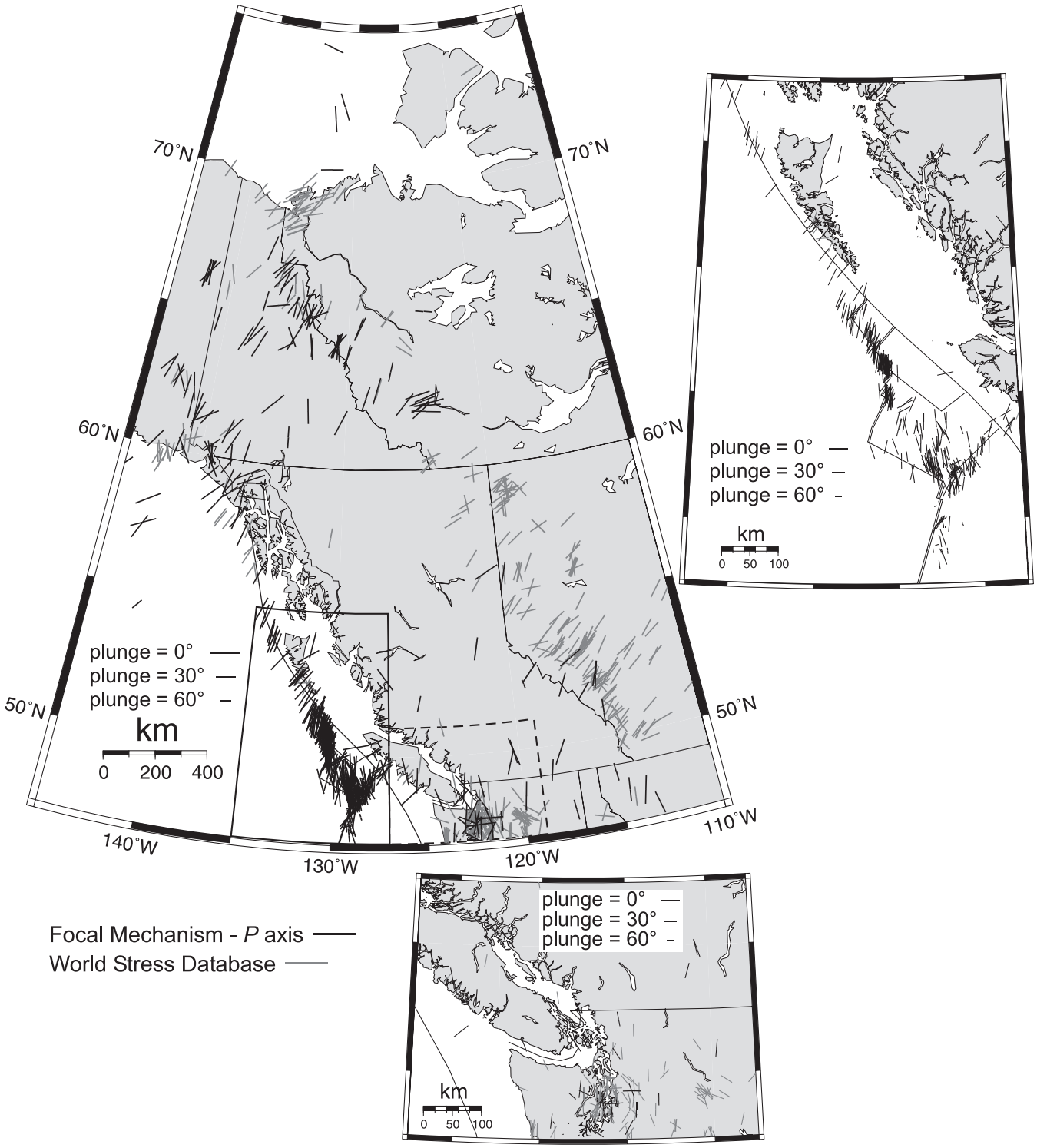

block, at the north end, the Oregon block, and the Sierra Nevada block to the south. Wells et al. (1998) concluded that rotation of these blocks results in extensional tectonics in the southwest United States with increasing north–south compression northward into western Washington and British Columbia.

Fig. 5. *T* axis azimuths from focal mechanisms in western Canada along with compressive stress directions from the world stress database. The arrow lengths are scaled according to the plunge of the axis with 0° plunge being the longest and 90° plunge having zero length.

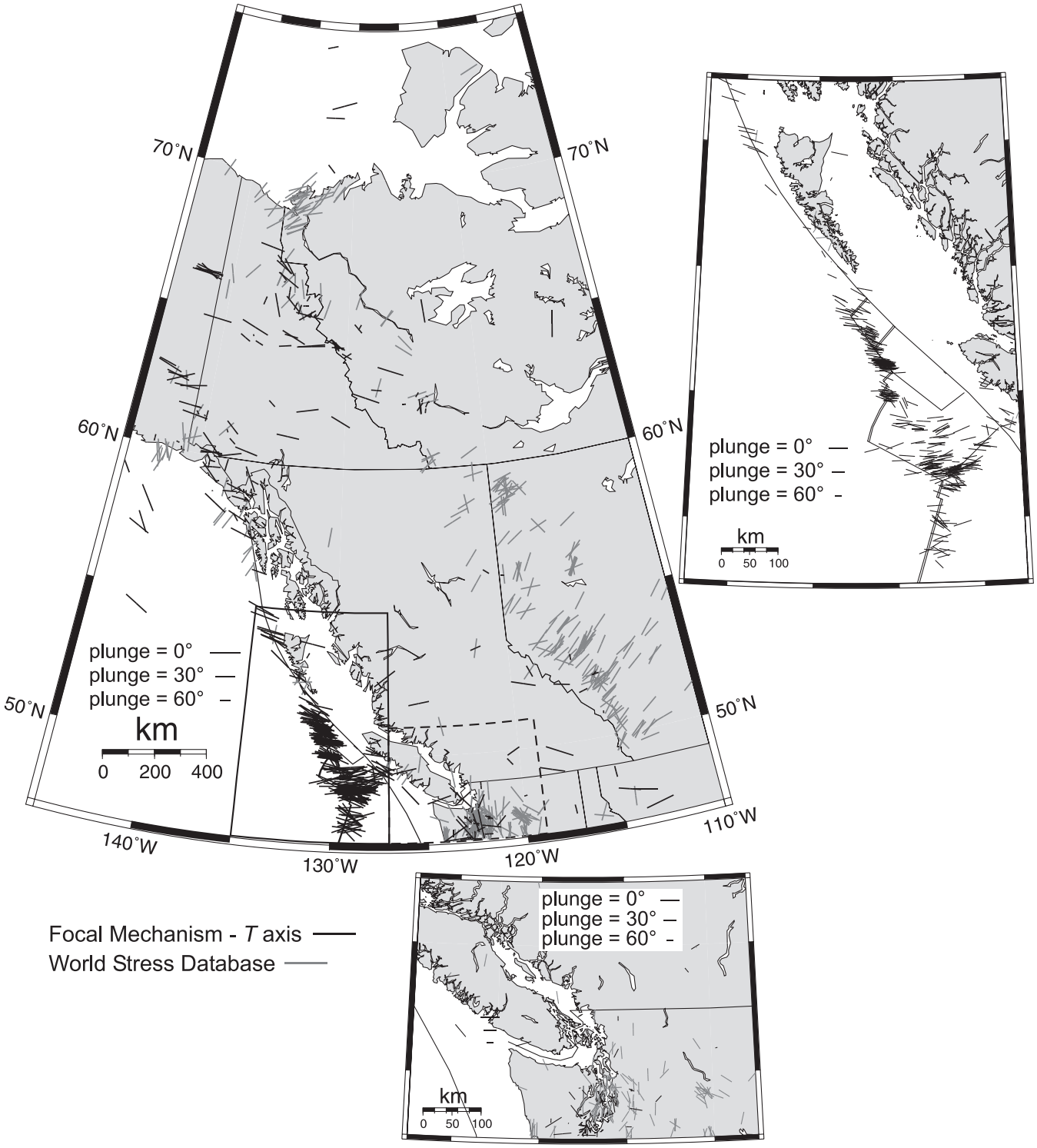

Northern Canadian Cordillera and Yakutat collision zone

More than 100 focal mechanisms have been calculated for earthquakes in the northern Canadian Cordillera and adjacent Yakutat collision zone. These include first-motion solutions for a few larger earthquakes prior to the mid-1970s (e.g., Cassidy and Bent 1993; Cassidy et al. 2002) and moment tensor solutions for a large number of events since the mid-1970s. The moment tensor solutions consist of 76 PGC RMT solutions and 23 Harvard CMT solutions. The focal mechanisms vary between strike-slip and thrust faulting across

Fig. 6. Focal mechanisms in the Mackenzie–Richardson mountains region. The focal mechanisms are mainly thrust faulting in the Nahanni region, a mixture of strike-slip and thrust faulting in the central and northern Mackenzie Mountains, and mainly strike-slip faulting in the Richardson Mountains. Ti F, Tintina Fault; FT B, Fold and Thrust Belt.

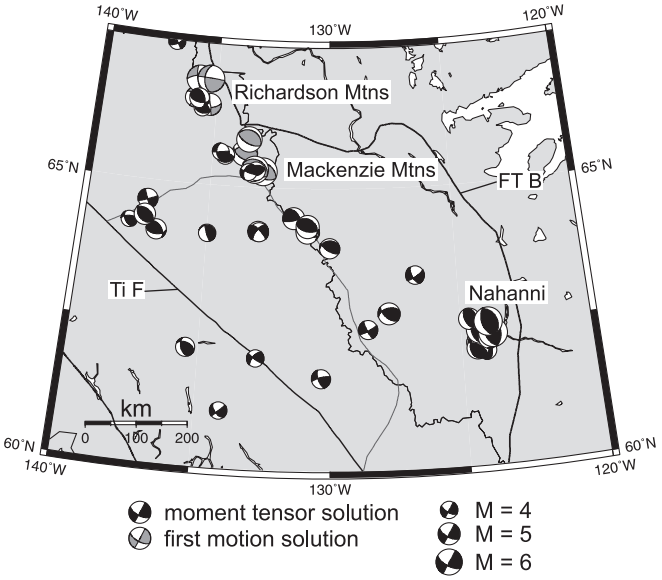

the northern Canadian Cordillera and through to the Yakutat collision zone, with a few normal faulting mechanisms also present. The Yakutat collision zone will be discussed separately from the northern Canadian Cordillera.

Northern Canadian Cordillera

Focal mechanisms

Focal mechanisms in the Mackenzie and Richardson mountains are a mixture of strike-slip and thrust mechanisms (Fig. 6). At the southern end of the Mackenzie Mountains, in the Nahanni region of the southwest Northwest Territories, the available focal mechanisms all show thrust faulting. This is the region of the 5 October and 23 December 1985 Nahanni earthquakes (M_w = 6.6 and 6.7, respectively). The central and northern Mackenzie Mountains have a mixture of strike-slip and thrust faulting mechanisms. A sequence of strong earthquakes (M = 6.0–6.5) occurred in this region in the mid-1950s, and first-motion solutions show thrust faulting along a shallow-dipping plane in a NNE–SSW direction (Cassidy et al. 2002). In the Richardson Mountains to the north, focal mechanisms become more dominantly strike-slip. First-motion solutions for a pair of large earthquakes (M = 6.0–6.5) in 1940 in the Richardson Mountains show strike-slip faulting along either a north–south or east–west plane (Cassidy and Bent 1993).

Stress analysis

Composite stress tensors are calculated for three regions in the northern Canadian Cordillera — the Richardson Mountains, the northern and central Mackenzie Mountains, and the Nahanni region (Fig. 7). Preliminary stress results for the northern Canadian Cordillera have been presented in Hyndman et al. (2005). The stress tensor results will be examined in more detail here. Figure 7 shows details of the stress tensors calculated for each region with the confidence limits represented by the distribution of small symbols around the large symbols. The confidence limits represent the 95% of the calculated stress tensors that are closest to the best answer (Michael 1987). The three principal stresses are $\sigma1$, $\sigma2$, and $\sigma3$, where $\sigma1 \geq \sigma2 \geq \sigma3$. One other parameter, ϕ, can also be calculated. ϕ is a measure of the relative sizes of the principal stresses and is defined by Angelier (1979) as

$$[1] \qquad \phi = \frac{\sigma2 - \sigma3}{\sigma1 - \sigma3}$$

Along the eastern mountain front, there is a change in the maximum compressive stress direction ($\sigma1$) between the Nahanni region (southern Mackenzie Mountains), the central and northern Mackenzie Mountains, and the Richardson Mountains (Fig. 7). In the Nahanni region (mainly thrust faulting), $\sigma1$ is in a ENE–WSW direction. The stress direction $\sigma1$ then changes to nearly north–south in the central and northern Mackenzie Mountains (mainly thrust faulting) and then to NE–SW in the Richardson Mountains (mainly strike-slip faulting).

The calculated stress tensors in Fig. 7 vary in quality depending on the number of focal mechanisms present in each grouping and whether they all have similar mechanisms or vary between strike-slip and thrust mechanisms. If there are few focal mechanisms or many with a similar mechanism, the computed confidence limits become large because of the inversion matrix becoming close to singular. This results in data fitting the best model very well; however, the large confidence limits would indicate that many other models could also fit the observed data equally well (Michael 1984). For data sets presented, here it is possible to give an estimate of the numerical value for the error of $\sigma1$ based on a visual inspection of the confidence limits; however, the confidence regions for $\sigma2$ and $\sigma3$ are too diffuse to estimate an error. In all of the data sets, the plunge of $\sigma1$ is near horizontal with an error of approximately ±10°–20° in the trend. Table 1 and subsequent tables list the estimated uncertainty for each data set.

In the Nahanni region, the data set consists of eight mechanisms, all of which are thrust faulting mechanisms with a similar slip direction. The resulting stress tensor (Fig. 7) has fairly large confidence limits for each of the principal stresses because of the similarity of the mechanisms. The Richardson Mountains data set is also small (six mechanisms) and dominated by strike-slip focal mechanisms. Therefore, the stress tensor also has large confidence limits (Fig. 7). In contrast, the data set for the central and northern Mackenzie Mountains is considerably larger (25 mechanisms) and consists of a mixture of strike-slip and thrust mechanisms. The stress tensor has a very well defined $\sigma1$ orientation with small confidence limits (Fig. 7). Table 1 summarizes the principal stress axes for the northern Cordillera.

The $\sigma1$ confidence limits for the central and northern Mackenzie Mountains do not overlap with the confidence limits for the Richardson Mountains or the Nahanni region, suggesting that $\sigma1$ for the central and northern Mackenzie Mountains is distinct from the other two regions. The $\sigma1$ confidence limits for the Richardson Mountains and the Nahanni region overlap only for a small range, which suggests that these two regions may also have compressive stress

Fig. 7. Compressive stress directions for the northern Canadian Cordillera and Yakutat collision zone. Dashed lines indicate the groupings of earthquakes used to calculate the stress tensors, and the arrows show the orientations of the maximum compressive stress ($\sigma 1$) and the *P* axis from the largest earthquakes in each group. With the exception of the central and northern Mackenzie Mountains, $\sigma 1$ and the *P* axis of the largest earthquakes in each group have very similar directions. Shown on the left and right hand sides are stress tensors calculated for each region, where $\sigma 1$, $\sigma 2$, and $\sigma 3$ are the principal stresses ordered from most compressional to most dilatational. Confidence limits are represented by the distribution of small symbols around the large symbols.

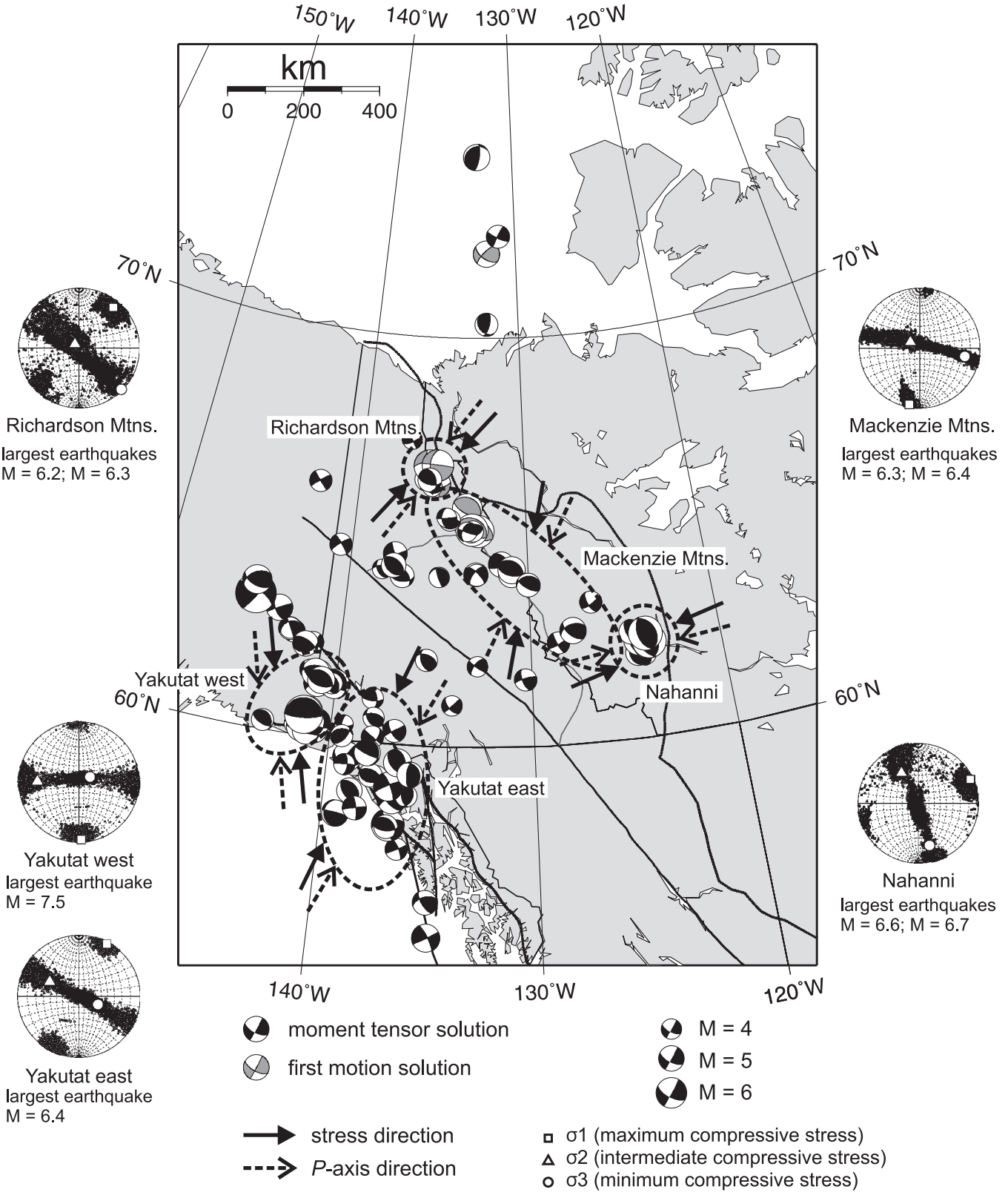

Table 1. Principal axes orientations for the northern Canadian Cordillera stress tensors.

	σ1		σ2		σ3		
Region	az [a]	pl	az	pl	az	pl	ϕ
YW	175±10	5	267	22	73	68	0.25
YE	26±15	5	292	38	122	52	0.27
Na	67±20	3	334	43	160	47	0.21
RM	43±15	10	225	81	133	0	0.10
MM	190±15	6	298	70	98	19	0.23

Note: YW, Yakutat west; YE, Yakutat east; Na, Nahanni region; RM, Richardson Mountains; MM, Mackenzie Mountains. σ1, σ2, and σ3 are the maximum, intermediate, and minimum principal stresses, respectively; ϕ, ratio of principal stresses (see text for details); az, azimuth (°); pl, plunge (°).

[a]For values in this column, errors estimated by a visual inspection of confidence limits.

directions that are distinct from one another. The ϕ value is ~0.2 for all the groupings with the exception of the Richardson Mountains (ϕ = 0.1). When ϕ is close to zero, σ2 and σ3 are approximately equal. This suggests that the state of stress is different in some way for the Richardson Mountains compared with the Mackenzie Mountains. However, the small and poorly constrained data set in the Richardson Mountains makes it difficult to draw any firm conclusions.

The σ1 stress axis can be compared with the *P* axis of the largest earthquakes in each region to see whether the compressive stress direction is consistent with the observed faulting. In the Richardson Mountains, the largest earthquakes are M = 6.2 and M = 6.3 and have similar focal mechanisms. The average *P* axis direction is almost identical to the compressive stress direction (Fig. 7). In the Nahanni region, the largest earthquakes are M = 6.6 and M = 6.7 and have similar focal mechanisms. The average *P* axis direction is also consistent with the compressive stress direction. In the central and northern Mackenzie Mountains region, the largest earthquakes are M = 6.3 and M = 6.4 and have similar focal mechanisms. The average *P* axis direction is rotated 16° clockwise relative to the compressive stress direction.

If there exists a dominant plane of weakness within a volume, slip can occur on the plane even if the compressive stress direction is at high angles to the fault. Therefore, if the largest earthquakes occur on faults that are mechanically weak, the compressive stress and *P* axis directions may be quite different from one another. In the Richardson Mountains and the Nahanni region, the compressive stress direction and the *P* axis direction for the largest earthquakes are similar. In the central and northern Mackenzie Mountains, it is more difficult to conclude whether the largest earthquakes have *P* axis directions that are significantly different from the compressive stress direction. The uncertainty on the *P* axis orientation is likely around 10° (e.g., Frolich and Davis 1999), which places it at the outer bounds of the confidence limits for σ1 (Fig. 7). If the difference is significant, then it suggests that the larger events rupture faults that are not optimally aligned for failure in the prevailing stress field and have low shear strength.

Fig. 8. Focal mechanisms in the Yakutat collision zone region. Focal mechanisms near the Yukon–Alaska border and to the west have primarily north–south-oriented *P* axes, while mechanisms to the east have NE–SW-trending *P* axes. De F, Denali Fault; Fa F, Fairweather Fault; QC F, Queen Charlotte Fault.

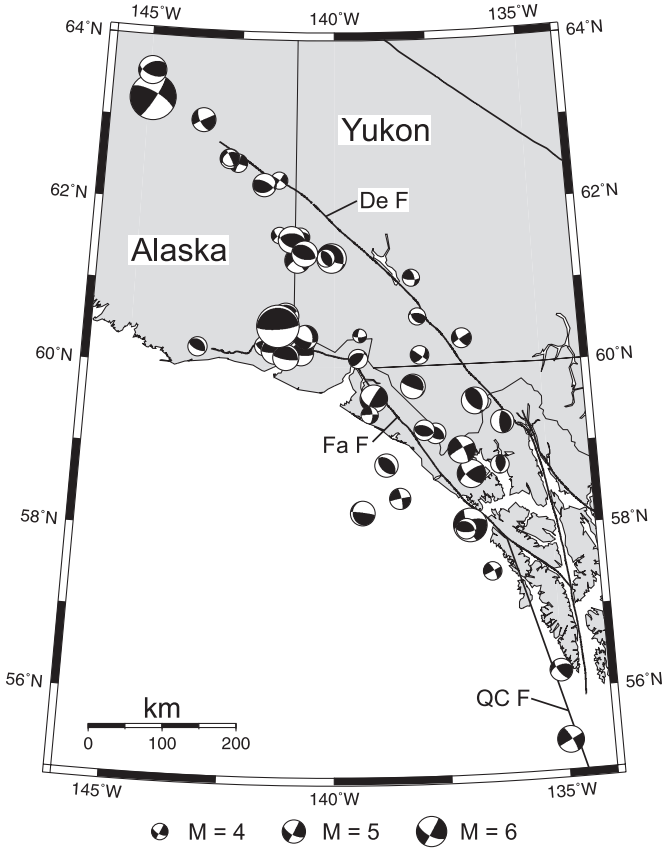

Yakutat collision zone

Focal mechanisms

In the vicinity of the Yakutat collision zone, a number of right lateral strike-slip and thrust faulting mechanisms are present (Fig. 8). This region is a transition zone from strike-slip motion along the Fairweather – Queen Charlotte fault in the southeast to oblique subduction along the Chugach – St. Elias thrust fault in the northwest. Global Positioning System (GPS) observations by Fletcher and Freymueller (1999) showed that the Yakutat block is moving in a northwest direction almost parallel to the Fairweather fault, but in a significantly more westerly direction than the Pacific plate. This results in some shortening along thrust faults in the Fairweather – Queen Charlotte fault region (Fletcher and Freymueller 1999).

The focal mechanisms are consistent with the relative motions of the Pacific and North America plates and with partitioning of the relative motion in the Yakutat collision zone (Doser and Lomas 2000). Along the Queen Charlotte and Fairweather faults motion is primarily strike-slip with the slip vectors parallel to the predicted Pacific – North America plate motions. (Doser and Lomas 2000). The Fairweather fault is considered the eastern boundary of the Yakutat block. Further to the north and west along the Fairweather

fault, the Yakutat block begins to collide directly with North America and the focal mechanisms become mainly thrust mechanisms. Numerous thrust faults are present, and the region experiences high rates of seismicity and rapid uplift in the St. Elias and Chugach Mountains region. The most recent major earthquake was the 1979 M_w = 7.5 earthquake, which apparently ruptured the plate interface between the North America and Pacific plates (Lahr et al. 1979; Estabrook et al. 1992). Further north, near the Denali fault, the focal mechanisms are predominately right lateral strike-slip with some thrust faulting. The 3 November 2002 M_w = 7.9 earthquake along the Denali fault in Alaska began as a thrust event with ~40 km of surface rupture and then ruptured ~218 km as a right lateral strike-slip event. Focal mechanisms for the larger aftershocks are a mixture of strike-slip, normal, and thrust mechanisms (Ratchkovski et al. 2003).

Stress analysis

The Yakutat collision zone data set is divided into two groups for the stress tensor analysis. The Yakutat west group consists mainly of thrust faulting mechanisms with north–south- or NE–SW-oriented *P* axes. The Yakutat east group is a mixture of strike-slip and thrust faulting mechanisms with NE–SW- to east–west-oriented *P* axes (Fig. 7; Table 1). In the Yakutat west group the compressive stress direction and the *P* axis orientation of the largest earthquake (M = 7.5) are almost identical. The compressive stress direction for the Yakutat east group is rotated 31° clockwise relative to the Yakutat west compressive stress direction. This is the region where the North America – Yakutat Block margin changes from north–south to east–west. Here, the compressive stress direction is also nearly identical to the *P* axis orientation of the largest earthquake (M = 6.4). However, there are several north–south-striking thrust faulting mechanisms present in the Yakutat east group, where the compressive stress and *P* axes directions are significantly different. This is consistent with the stress field in the Yakutat collision zone changing steadily from east–west in the Alaska panhandle region to north–south in eastern Alaska. This shows that, in a complex tectonic setting like the Yakutat collision zone, it is not reasonable to infer a regional stress field by combining large groups of focal mechanisms.

Southern Canadian Cordillera

Focal mechanisms

Prior to having the capability to calculate RMT solutions, focal mechanisms in the southern Canadian Cordillera were scarce. The first focal mechanism calculated in the southern Canadian Cordillera was for the 14 May 1978 M_L (local magnitude) = 4.8 earthquake near McNaughton Lake (Rogers et al. 1980). With the ability to calculate RMT solutions, more than 20 moment tensor solutions have been calculated for the southern Canadian Cordillera in recent years. Focal mechanisms in the southern Canadian Cordillera show mostly thrust faulting north of around 50°N (Fig. 9), indicating a compressional tectonic regime consistent with the major geological features in the area. No normal faulting RMT solutions have been calculated for the southern Canadian Cordillera, which suggests that there is no active extensional tectonics in this region. This contrasts markedly with focal mechanisms from the western United States, just south of the Canada – United States border, which show normal faulting corresponding to an extensional tectonic regime. In the vicinity of the Canada – United States border is a transition zone from compressional tectonics in western Canada to extensional tectonics in the western United States (e.g., Sbar et al. 1972; Zoback and Zoback 1980). In the Canada – United States border region, the RMT solutions are strike-slip and thrust faulting mechanisms (Fig. 9) and have *P* axes oriented approximately north–south through to the eastern Cordillera.

Stress analysis

Focal mechanisms in the southern Canadian Cordillera are a mixture of strike-slip and thrust mechanisms, which means the stress tensor should be fairly well constrained. The stress tensor calculated using all of the focal mechanisms for the southern Canadian Cordillera is shown at the bottom of Fig. 9 and details are listed in Table 2. As was the case in the northern Cordillera, $\sigma 1$ is near horizontal with an approximate ±10°–15° in the trend. The calculated stress tensor has a well-constrained $\sigma 1$ oriented in a NNE–SSW direction. The $\sigma 2$ and $\sigma 3$ values overlap considerably, which is expected with a mixture of strike-slip and thrust mechanisms.

By a visual inspection of the focal mechanisms in Fig. 9 and the *P* axis azimuths in Fig. 4, there appears to be a difference in the compressive stress direction between focal mechanisms located north and south of 51°N. The maximum compressive stress direction appears to be NE–SW or NNE–SSW north of around 51°N and north–south south of around 51°N. The focal mechanisms are divided into two groups based on latitude, and stress tensors were calculated to compare the principal stress orientations (Fig. 9). The circled focal mechanism in Fig. 9 has a mechanism more consistent with the southern group of events but geographically is closer to the northern group. For the purposes of the stress tensor analysis the circled mechanism is placed with the southern group. Grouping the circled mechanism with the northern events has little effect on the results; therefore, only one set of results is presented here.

The maximum compressive stress direction is well defined for both the northern and southern groups (Fig. 9). The $\sigma 1$ value for the stress tensor calculated for the northern group has an azimuth of 30° compared with a $\sigma 1$ azimuth of 2° for the southern group. The $\sigma 1$ confidence limits do not overlap for the two groups, indicating they are distinct from one another. On the basis of these results, there appears to be a sharp latitudinal transition from north–south to NE–SW compression in southern British Columbia at around 51°N.

Focal mechanisms from the northwestern United States are consistent with east–west or NE–SW extensional tectonics (e.g., Sbar et al. 1972; Zoback and Zoback 1980; Stickney and Bartholomew 1987; Braunmiller 1998; Stickney and Lageson 2002) compared with north–south or NE–SW compression in western Canada. Sbar et al. (1972) calculated composite first-motion focal mechanisms for microearthquakes from southwestern Utah to northwestern Montana and suggested that the tectonic character of this region is east–west extension. Zoback and Zoback (1980) also suggested an east–west extensional stress regime for the western Montana and western Wyoming region. Braunmiller (1998) calculated

Fig. 9. Moment tensor solutions calculated for the southern Canadian Cordillera. North of around 51°N the mechanisms are mainly thrust faulting mechanisms consistent with compressional tectonics. The solutions then change to strike-slip faulting around the Canada – United States border. The circled mechanism is singled out for further analysis (see text). Composite stress tensors are shown along the bottom for all focal mechanisms (left), focal mechanisms north of 51°N (middle), and focal mechanisms south of 51°N (right). There is a change in σ1 from NE–SW north of 51°N to north–south south of 51°N. OSU, Oregon State University; PGC, Pacific Geoscience Centre.

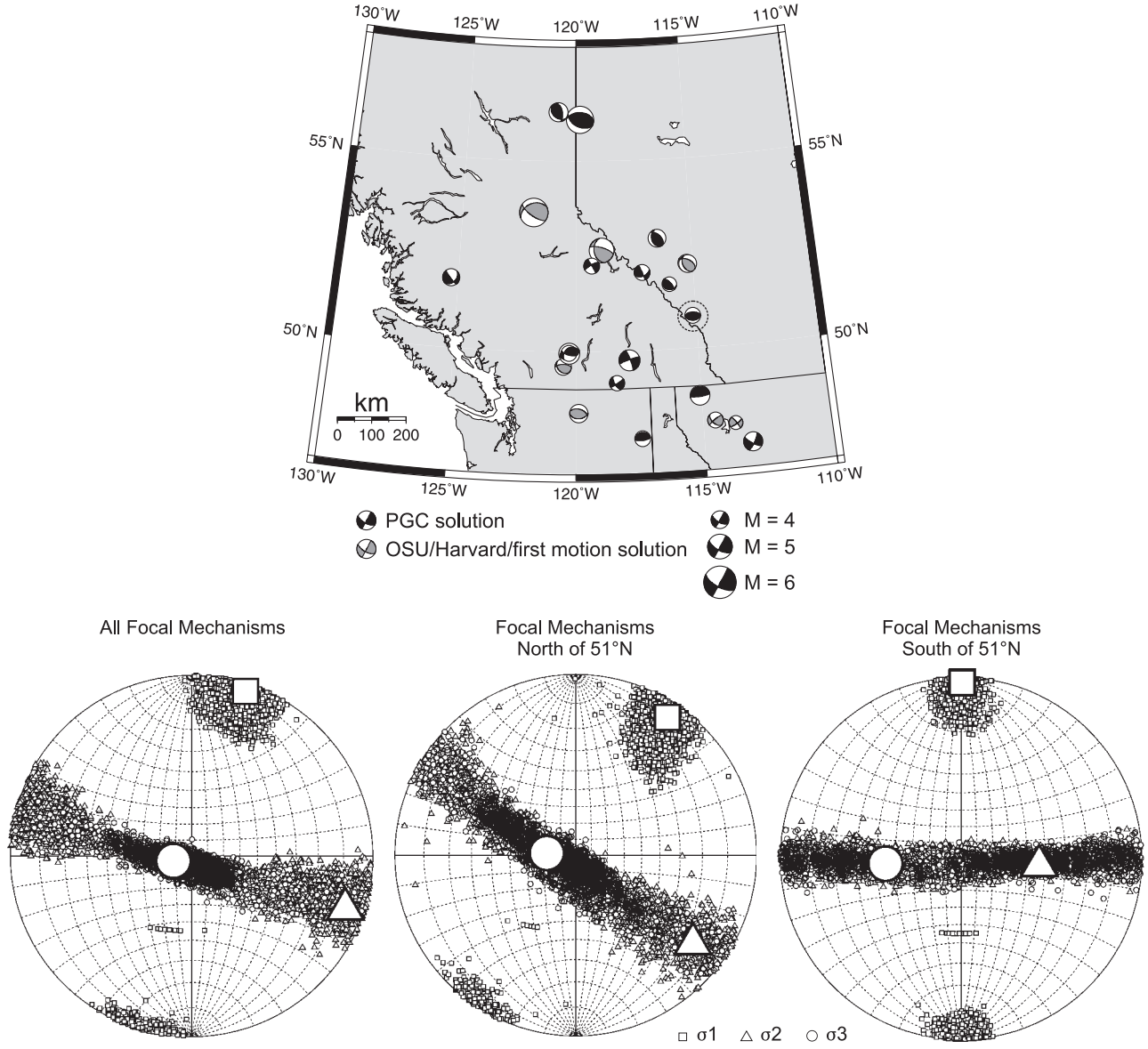

a number of RMT solutions for the western United States, which show normal faulting with an east–west tension axis for the western Wyoming – southeastern Idaho region and NE–SW tension for central Idaho. Stickney and Bartholomew (1987) proposed a NE–SW tensional tectonic regime for southwest Montana and adjacent Idaho. Stickney and Lageson (2002) presented a RMT solution calculated by John Nábělek at OSU for a M_w = 4.8 event in southwest Montana, which was a normal faulting mechanism with a NE–SW tension axis.

The abovementioned results demonstrate that near the Canada – United States border the tectonic setting becomes unclear. The three RMT solutions in northwestern Montana (Fig. 9) are strike-slip mechanisms with east–west tension and north–south compression. As well, there are two more strike-slip mechanisms in southeastern British Columbia near the Canada – United States border with east–west tension and north–south compression. The current tectonics of the border region represents a combination of transition from extensional tectonics in the south to compression in the north, coupling of the Juan de Fuca plate with the North America plate, and rotation of the Washington and Oregon fore-arc blocks. On the basis of focal mechanisms alone, it is not possible to determine which is the dominant force in southeastern British Columbia and northwest Montana.

Exactly where the transition from compressional to extensional tectonics occurs is important for seismic hazard estimates in western Canada. If the compressional tectonic setting extends south to the Canada – United States border, then southern British Columbia and southern Alberta (includ-

Table 2. Principal axes orientations for the southern Canadian Cordillera stress tensors.

	σ1		σ2		σ3		
Region	az [a]	pl	az	pl	az	pl	ϕ
All Mechanisms	17±15	6	108	10	257	79	0.20
North of 51°N	30±15	9	123	19	275	69	0.14
South of 51°N	2±10	5	96	42	267	48	0.04

Note: σ1, σ2, and σ3 are the maximum, intermediate, and minimum principal stresses, respectively; ϕ, ratio of principal stresses (see text for details); az, azimuth (°); pl, plunge (°).

[a]For values in this column, errors estimated by a visual inspection of confidence limits.

ing the Calgary area) may be at risk for large thrust-style earthquakes similar to the 1985 Nahanni events in the Northwest Territories. If the compressional to extensional tectonics transition occurs further north, then the seismic hazard from large thrust earthquakes is lower for southern British Columbia and southern Alberta. There is evidence for extensional tectonics in southern British Columbia, which includes Eocene (~55 Ma) normal faults and high-grade gneiss complexes (see Glombick et al. 2006; Parrish et al. 1988). However, no geologic evidence has been found for more recent episodes of extension in southern British Columbia. With the presently available RMT solutions, it is not possible to determine where the compressional to extensional tectonics transition occurs. However, they do suggest that given another decade or two there may be enough moment tensor solutions to give a clearer picture of the contemporary tectonic setting of the southern Canadian Cordillera.

Vancouver Island – Puget Sound

Focal mechanisms

The Vancouver Island – Puget Sound region is a tectonically complex region where the Juan de Fuca plate is subducting obliquely beneath the North America plate. The strike of the margin changes from north–south around southern Washington to NW–SE in the vicinity of Vancouver Island. First-motion mechanisms for small earthquakes occurring within the overlying plate and the subducting slab are mainly a mixture of strike-slip and thrust faulting in the overlying plate (Mulder 1995), and strike-slip and normal faulting within the subducting slab (Bolton 2003), with no obvious pattern in the strike of the fault planes in either case. The maximum compressive stress direction as determined from first-motion solutions is margin parallel in the overlying crust (Mulder 1995), and the maximum tensional stress direction in the subducting slab is oriented east–west (downdip tension; Bolton 2003). Thirty-eight RMT solutions are available for the Vancouver Island – Puget Sound region, calculated in this study and by OSU (Fig. 10).

Stress analysis

As is the case with the first-motion mechanisms, the RMT solutions show no obvious pattern in faulting style, reflecting the complex tectonic setting. The RMT solutions can be divided into events occurring within the overlying crust (Fig. 10, top) and those occurring within the subducting slab (Fig. 10, bottom). The light grey events in Fig. 10 (top) have

Fig. 10. RMT solutions for the Vancouver Island – Puget Sound region. No obvious pattern in the strike of the fault planes is evident, reflecting the complex tectonic setting. (Top) RMT solutions for events located in the overlying crust. The two light grey mechanisms are events that may be either crustal or in-slab events and have been grouped with the crustal events for the purpose of the stress analysis. (Bottom) RMT solutions for events located within the subducting slab.

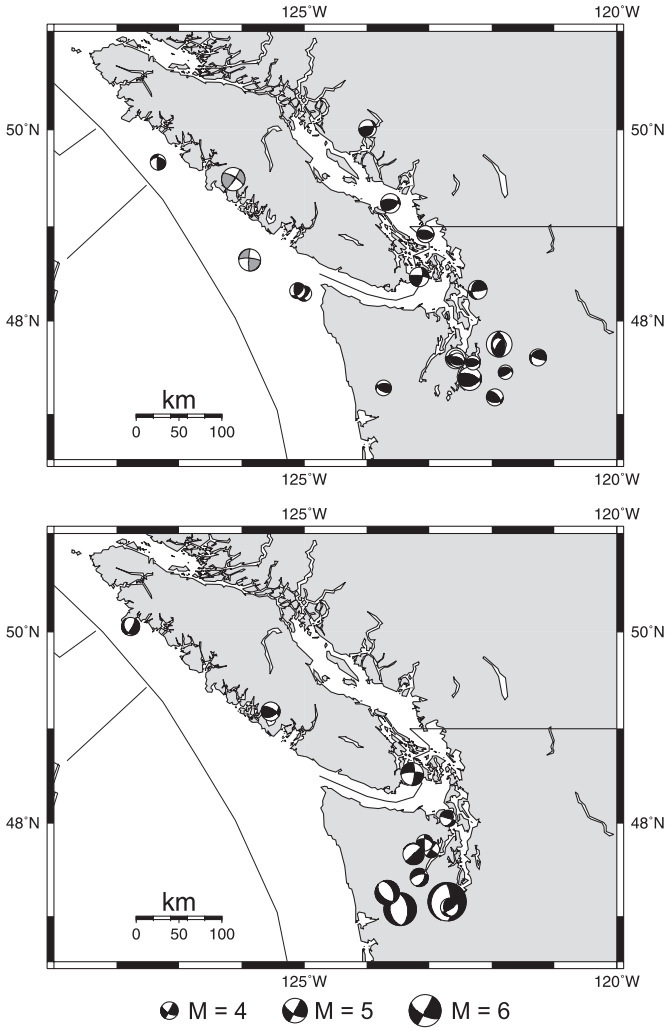

depths of 27 km and 33 km, and it is uncertain whether they are located in the overlying crust or in the subducting slab. Whether these events are considered as overlying crust or in-slab events has no significant effect on the stress tensor results. For the purposes of the stress analysis, they are grouped with the crustal events. The stress tensor for the overlying crust events (Fig. 11, left) has poorly constrained σ1 and σ2 axes. However, the best fitting σ1 orientation is margin parallel (NW–SE in the Vancouver Island region), which is consistent with Mulder (1995). The stress tensor for the in-slab events (Fig. 11, right) is very poorly constrained. The best fitting tension axis (σ3) is oriented east–west, which is consistent with Bolton (2003) and with downdip tension.

Fig. 11. Composite stress tensors from RMT analysis in the Vancouver Island – Puget Sound region. (Left) Stress tensor for the overlying crust events with σ1 oriented margin parallel. Also shown is separate stress tensor plots for each of the principal axes. (Right) Stress tensor for the in-slab events with σ3 oriented in the downdip direction. Also shown is separate stress tensor plots for each of the principal axes.

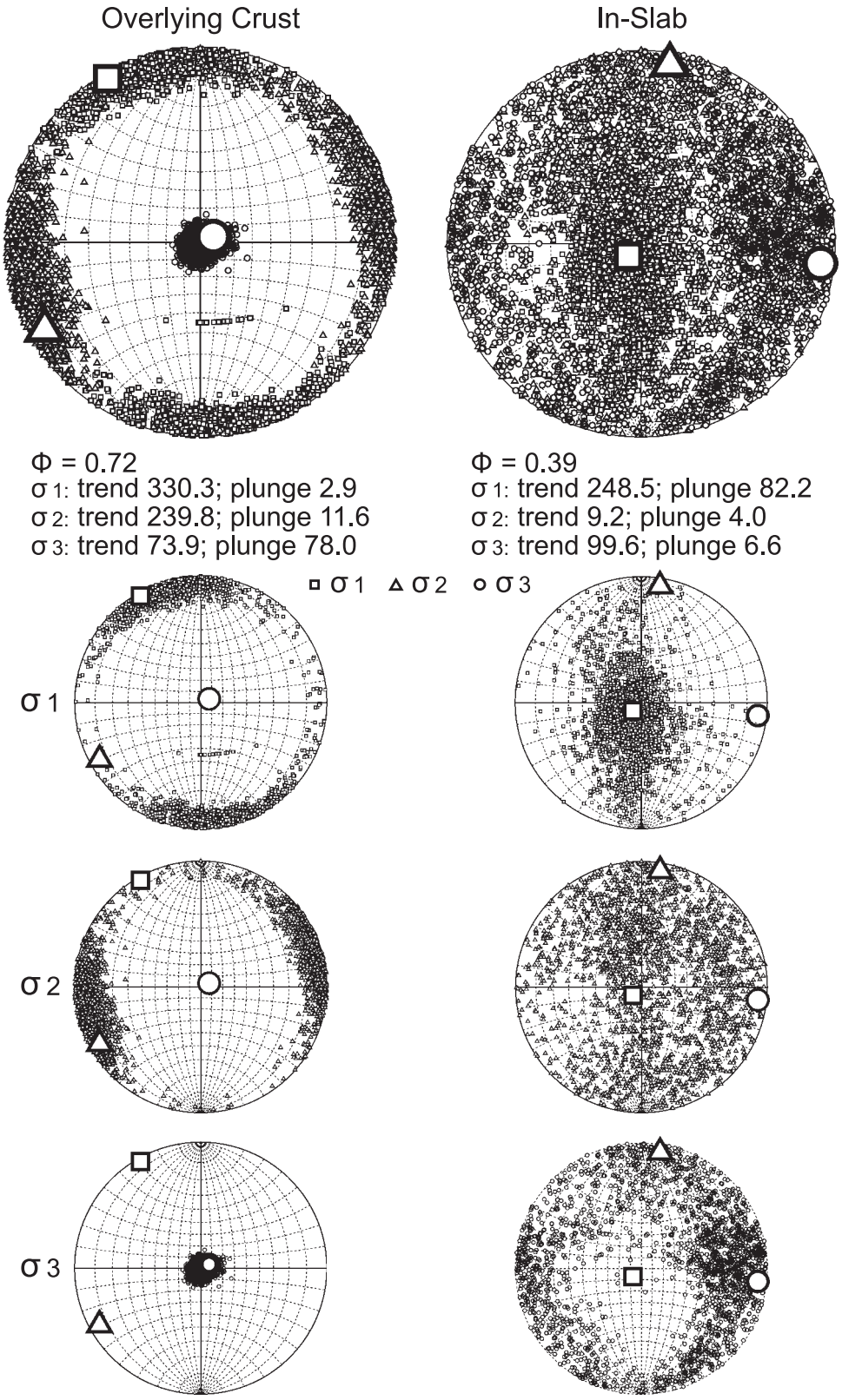

Fig. 12. Moment tensor and first-motion solutions (Bird 1997) for the Queen Charlotte Islands region. The thick black lines indicate the approximate trend of the Queen Charlotte fault in the southern and northern Queen Charlotte Islands region. The large grey arrow is the direction of Pacific – North America (PA/NA) motion. The moment tensor solutions are strike-slip in the northern Queen Charlotte fault region and thrust in the southern Queen Charlotte fault region. The first-motion mechanisms are a mixture of thrust, normal, and strike-slip mechanisms.

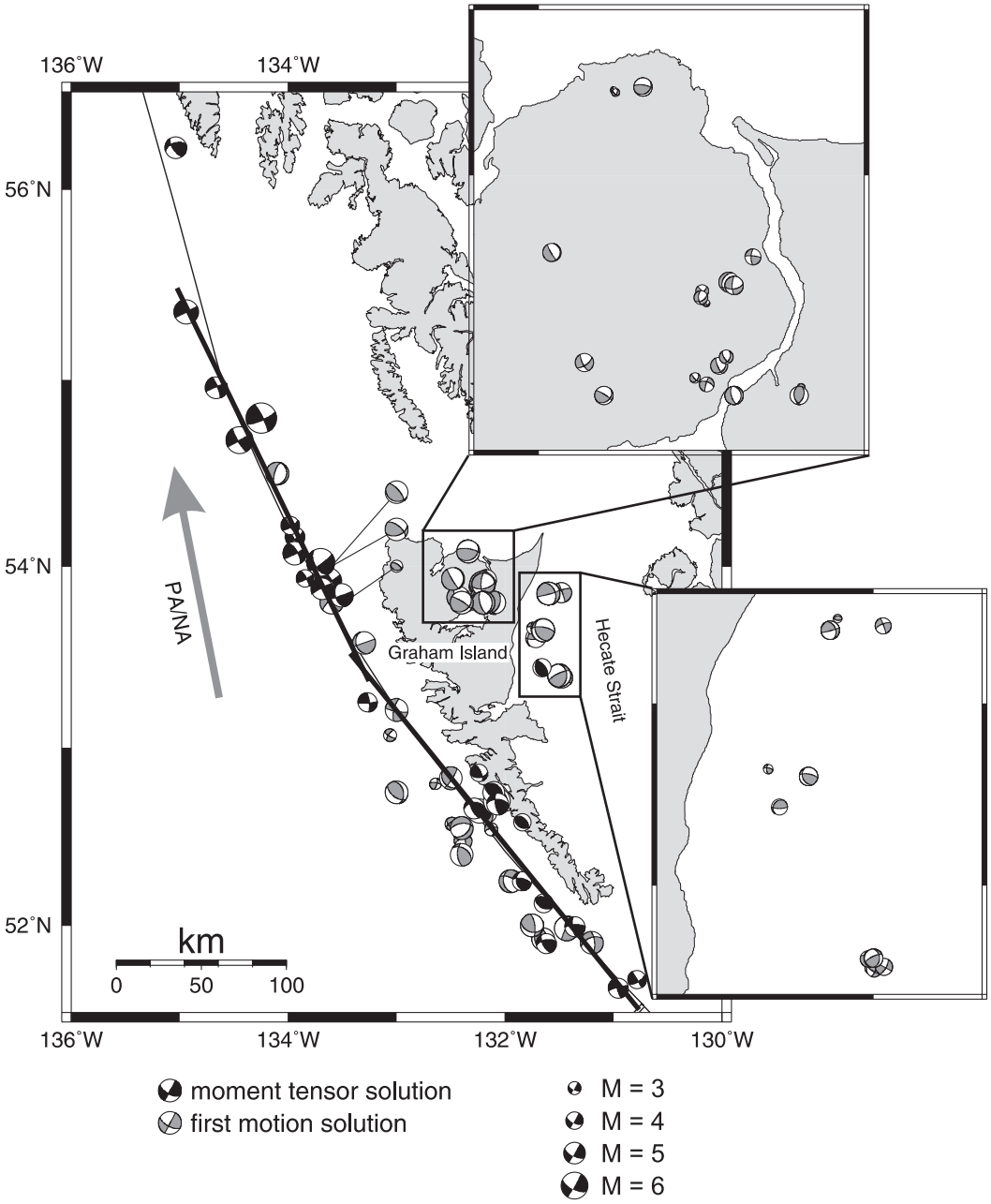

Queen Charlotte Islands

Focal mechanisms

Fifteen RMT solutions and one Harvard CMT have been calculated along the Queen Charlotte fault (Fig. 12). In the northern Queen Charlotte Islands, the moment tensor solutions are strike-slip, some with a small thrust component, and are consistent with the strike of the Queen Charlotte fault. In the southern Queen Charlotte Islands, the moment tensor solutions are consistently thrust mechanisms on high-angle faults, some with a small strike-slip component.

It has been known for some time that a component of convergence between the Pacific and North America plates exists in the Queen Charlotte Islands region (e.g., Riddihough and Hyndman 1989; Bérubé et al. 1989), and recent GPS results from the Queen Charlotte Islands region show convergence between the Pacific and North America plates (Mazzotti et al. 2003*b*). However, the amount of thrust faulting present in the southern Queen Charlotte Islands, as shown by the RMT solutions, represents an important new result. Two models have been proposed to describe how convergence is accommodated in the Queen Charlotte Islands region.

Northern Queen Charlotte Fault
Moment Tensor Solutions

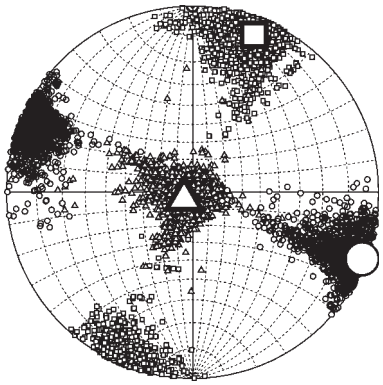

Φ = 0.48
σ1: trend 18.2; plunge 10.1
σ2: trend 205.8; plunge 79.7
σ3: trend 108.3; plunge 1.3

Southern Queen Charlotte Fault
Moment Tensor Solutions

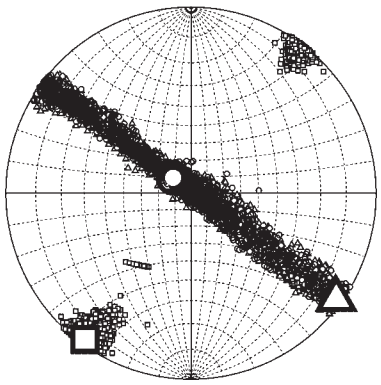

Φ = 0.10
σ1: trend 216.3; plunge 0.8
σ2: trend 126.0; plunge 4.9
σ3: trend 316.0; plunge 85.0

Northern Queen Charlotte Fault
First Motion Solutions

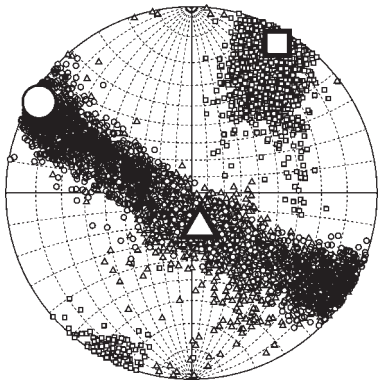

Φ = 0.24
σ1: trend 32.7; plunge 9.4
σ2: trend 191.4; plunge 79.8
σ3: trend 302.1; plunge 3.6

Southern Queen Charlotte Fault
First Motion Solutions

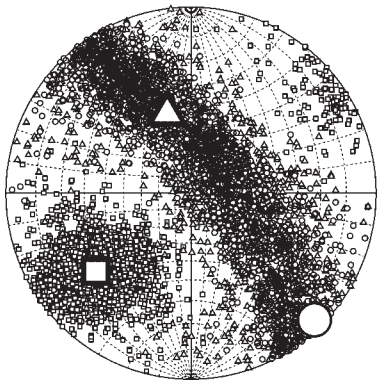

Φ = 0.17
σ1: trend 227.4; plunge 25.5
σ2: trend 43.1; plunge 64.4
σ3: trend 136.4; plunge 1.6

Northern Queen Charlotte Fault
All Solutions

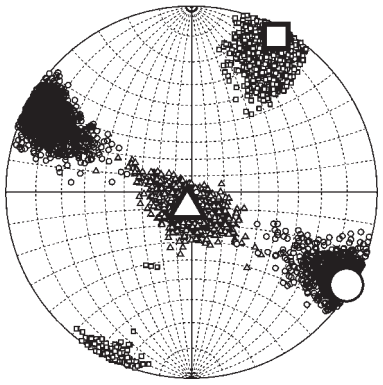

Φ = 0.43
σ1: trend 27.3; plunge 9.7
σ2: trend 213.1; plunge 80.2
σ3: trend 117.4; plunge 0.9

Southern Queen Charlotte Fault
All Solutions

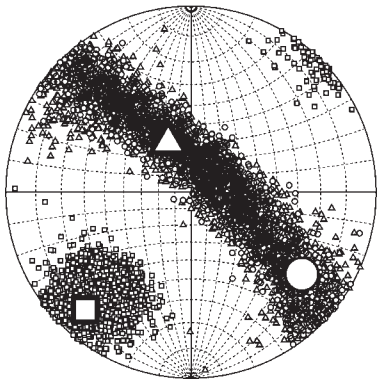

Φ = 0.07
σ1: trend 220.2; plunge 18.0
σ2: trend 347.8; plunge 61.9
σ3: trend 122.9; plunge 20.7

□ σ1 △ σ2 ○ σ3

Fig. 13. Stress tensors calculated for the northern and southern Queen Charlotte fault segments using moment tensor solutions (top), first-motion solutions (middle), and both moment tensor and first-motion solutions (bottom). For the northern Queen Charlotte fault segment,σ1 is oriented ~45° to the strike of the fault, and for the southern segment, σ1 is oriented ~80° to the strike of the fault. These stress tensors are calculated using focal mechanisms that are located on the Queen Charlotte fault and may not represent the true nature of the regional stress field in the Queen Charlotte Islands region due to Pacific – North America motion.

Oblique underthrusting of the Pacific plate beneath the continental margin is suggested by the presence of an accretionary sedimentary prism that includes compressive structures and folding; a deep trough with depressed oceanic crust and bathymetric high, which suggests flexural bending; and uplift along the margin of the Queen Charlotte Islands with simultaneous subsidence of the Hecate Strait trough (e.g., Hyndman and Hamilton 1993; Riddihough and Hyndman 1989; Hyndman and Ellis 1981). Convergence may also be accommodated by internal deformation and shortening of both the Pacific and North America plates without underthrusting of the Pacific plate, as suggested by Rohr et al. (2000) based on seismic reflection data. GPS results from Mazzotti et al. (2003*b*) provide strong constraints on the convergence distribution in the Queen Charlotte Islands region but cannot discriminate between the two models.

In addition to the moment tensor solutions, Bird (1997) calculated 35 first-motion solutions for small earthquakes in the vicinity of the Queen Charlotte fault (Fig. 12). These solutions are a mixture of single event solutions and composite focal mechanisms. Bird (1997) also calculated 28 first-motion mechanisms for the Graham Island region and 29 first-motion mechanisms for the Hecate Strait region, which are also a mixture of single event and composite focal mechanisms (Fig. 12). The first-motion solutions in the vicinity of the Queen Charlotte fault are a mixture of thrust, normal, and strike-slip faulting (Fig. 12) (Bird 1997; Bérubé et al. 1989). Some are consistent with the strike of the Queen Charlotte fault, and others appear to have no relation to the fault strike. Most of the first-motion solutions are for much smaller magnitude events than the moment tensor solutions and may be occurring on small subsidiary faults. In the Graham Island and Hecate Strait regions, the first-motion solutions also show a mixture of thrust, normal, and strike-slip faulting (Fig. 12).

Stress analysis

The Queen Charlotte fault

The Queen Charlotte fault changes strike between the southern and northern Queen Charlotte Islands region. The strike changes from a NW–SE strike (~320°) in the south to a NNE–SSW strike (~335°) (thick black lines in Fig. 12) and becomes even more northerly north of the Queen Charlotte Islands region. The most northerly segment had almost no focal mechanisms associated with it during the period of this study and will not be discussed here. Stress tensors can be calculated for events along the Queen Charlotte fault to investigate the consistency of the principal stresses with the strike of the fault.

For the purposes of calculating stress tensors, the dividing line between the northern and southern Queen Charlotte fault is chosen as 53°N. Moment tensor solutions north of 53°N are strike-slip mechanisms, while those south of 53°N are primarily thrust mechanisms. In the northern Queen Charlotte fault region, the earthquakes are strike-slip and appear to rupture the fault. These events reflect northward motion of the Pacific plate relative to the North America plate. In the southern Queen Charlotte fault region, the earthquakes are mainly thrust mechanisms and appear to occur on high-angle faults adjacent to the Queen Charlotte fault. The number of thrust faulting mechanisms calculated in a relatively short period of time indicates a significant amount of convergence between the Pacific and North America plates. The lack of low-angle thrust faulting suggests that the thrust faulting is related to deformation within the North America plate and not underthrusting of the Pacific plate.

The stress tensor calculated using moment tensor solutions in the northern Queen Charlotte Islands region has a σ1 of 18° (Fig. 13, top left). This gives an angle of 43° with the northern segment of the Queen Charlotte fault, which is consistent with the maximum shear stress of 45° on a fault. The stress tensor for the southern segment of the Queen Charlotte fault calculated using moment tensor solutions has σ1 with an azimuth of 36° (Fig. 13, top right). This gives an angle of 76° with the southern segment of the Queen Charlotte fault. Along the southern segment of the Queen Charlotte fault, the mechanisms are mainly thrust faulting with a small strike-slip component, which means that the *P* axis orientation should be close to, but not quite, 90°. The orientation of σ1 with the southern segment of the Queen Charlotte fault is consistent with the *P* axis orientation for fault mechanisms along the southern Queen Charlotte fault segment.

Stress tensors calculated using the first-motion solutions are shown in Fig. 13 (middle). Bird (1997) assigned a quality factor to the first-motion solutions on a scale from 0 (very good) to 3 (poor). These are used to weight the solutions in the stress tensor calculations. The confidence limits are large, particularly for the southern Queen Charlotte fault segment. In the southern Queen Charlotte fault region, the first-motion mechanisms consist of normal, thrust, and strike-slip faulting with no consistent *P* axis orientation. Therefore, it is not possible to calculate a well-constrained stress tensor. The orientation of σ1 is consistent with the moment tensor results for the southern Queen Charlotte fault segment within the confidence limits. Bird (1997) calculated the average *P* axis direction from the first-motion mechanisms for the entire Queen Charlotte fault (Table 3). The *P* axis orientation is midway between σ1 for the northern and southern Queen Charlotte fault segments calculated using first-motion solutions (Table 3). Calculating the stress tensor using all of the Queen Charlotte fault first-motion solutions results in a σ1 that is almost identical with Bird (1997) (Table 3).

Combining all of the mechanisms together results in the stress tensors in Fig. 13 (bottom). For the northern Queen Charlotte fault σ1 is oriented 52° with respect to the fault strike. Some of the first-motion solutions for the northern Queen Charlotte fault segment are thrust mechanisms that change the orientation of the σ1 with respect to the fault.

Table 3. Average *P* axis orientation (°) (Bird 1997) compared with F1 for the Queen Charlotte fault.

	EQCF	NQCF	SQCF
Bird (1997)	39±13	–	–
This study	41±20 [a]	33±15 [a]	47±20 [a]

Note: EQCF, entire Queen Charlotte fault; NQCF, northern Queen Charlotte fault; SQCF, southern Queen Charlotte fault.
[a]Errors estimated by a visual inspection of confidence limits.

The orientation is still within the confidence limits of being 45° to the strike of the fault. For the southern Queen Charlotte fault segment, σ1 is oriented 80° with respect to the fault strike, which is very close to the moment tensor results. It should be noted that these results combine data sets from events that are influenced by the Queen Charlotte fault (moment tensor solutions) with events that may or may not be related to the Queen Charlotte fault (first-motion solutions from much smaller earthquakes). Therefore, it may not be reasonable to infer stress information from a combination of data sets.

Graham Island and Hecate Strait

Earthquakes in the Graham Island and Hecate Strait regions are influenced by Pacific – North America motion but are not directly related to the Queen Charlotte fault. Stress tensor analysis was carried out on the focal mechanisms to see what information could be extracted (Fig. 14), and details are listed in Table 4.

The stress tensor for the events in the Graham Island region (Fig. 14, top) has σ1 with a more NE–SW orientation compared with events in the Hecate Strait region (Fig. 14, middle). The σ2 and σ3 values are also similar in magnitude in the Graham Island region, as indicated by the low value of ϕ. In the Hecate Strait region, the magnitudes of σ2 and σ3 are quite different. Combining the two data sets gives σ1 with an orientation midway between the σ1 orientations for the separate data sets (Fig. 14, bottom). The magnitude of σ2 and σ3 are very distinct from one another, similar to the Hecate Strait results.

Bird (1997) calculated average *P* axis orientations for the Graham Island and Hecate Strait regions from the first-motion focal mechanisms. Table 5 compares the average *P* axis orientations with the σ1 orientations derived from the stress tensor inversions. The results agree very well within the uncertainties, and the stress tensor results support those of the Bird (1997).

The σ1 results for the Graham Island and Hecate Strait regions agree within the uncertainties. As well, the *P* axis orientations for Graham Island and Hecate Strait obtained by Bird (1997) agree within the uncertainties. Therefore, it seems reasonable to use the stress tensor from the combined Graham Island and Hecate Strait data sets to represent the stress field for the Graham Island – Hecate Strait region (Fig. 14).

Comparison with the San Andreas fault

The San Andreas fault can serve as a useful analogy for the Queen Charlotte fault. Like the Queen Charlotte fault, the San Andreas fault forms a boundary where the Pacific plate is moving north relative to the North America plate. The San Andreas fault is one of the most intensively studied

Table 4. Principal axes orientations for the Graham Island – Hecate Strait stress tensors.

	σ1		σ2		σ3		
Region	az [a]	pl	az	pl	az	pl	ϕ
GI	34±15	26	177	58	295	16	0.07
HS	189±15	16	50	69	283	13	0.32
GI–HS	20±20	10	138	70	287	17	0.33

Note: GI, Graham Island; HS, Hecate Strait; σ1, σ2, and σ3 are the maximum, intermediate, and minimum principal stresses, respectively; ϕ, ratio of principal stresses (see text for details); az, azimuth (°); pl, plunge (°).
[a]For values in this column, errors estimated by a visual inspection of confidence limits.

Table 5. Average *P* axis orientation (°) (Bird 1997) compared with σ1 for the Graham Island (GI) and Hecate Strait (HS) regions.

	GI	HS	GI–HS
Bird (1997)	26±7	12±17	–
This Study	34±20 [a]	9±20 [a]	20±15 [a]

[a]Errors estimated by a visual inspection of confidence limits.

fault systems in the world and thousands of fault plane solutions have been calculated for events occurring along, or associated with, the fault (e.g., Provost and Houston 2003).

A number of studies have examined the state of stress along the San Andreas fault (e.g., Townend and Zoback 2001; Townend and Zoback 2004; Provost and Houston 2001; Provost and Houston 2003; Hardebeck and Hauksson 2001; Jones 1988). Provost and Houston (2001) looked at the stress field along the creeping portion of the San Andreas fault in central California. They found that the maximum principal stress is oriented at high angles of up to 80° to the strike of the fault and interpreted this as suggesting that the San Andreas fault is mechanically weak. Provost and Houston (2003) studied the stress field of the San Andreas fault in the San Francisco Bay Area and northern California. They found that the angle between the San Andreas fault and the maximum compressive stress direction is around 55° in this region and suggested that the northern part of the fault is stronger with greater frictional strength than the southern creeping portion. Townend and Zoback (2001, 2004), Hardebeck and Hauksson (2001), and Jones (1988) also found that the maximum compressive stress is at high angles with the San Andreas fault and interpreted this as a mechanically weak fault. High frictional strength along the San Andreas fault should result in a local heat flow anomaly along the fault, but none has been found, which also suggests a weak fault (e.g., Brune et al. 1969; Lachenbruch and Sass 1992; Saffer et al. 2003). A recent study (Hardebeck and Michael 2004) suggests that the maximum principal stress may be at intermediate angles to the San Andreas fault and other factors may be involved in making the fault appear to be weak (e.g., having a coefficient of friction half that of a strong fault or containing pore fluids at elevated pressure).

Compared with the San Andreas fault region, there are relatively few focal mechanisms available for the Queen Charlotte fault and Queen Charlotte Islands region. One pos-

Fig. 14. Compressive stress directions (arrows) for the northern and southern Queen Charlotte fault segments and the Graham Island – Hecate Strait region. Dashed lines indicate the groupings of earthquakes used to calculate the stress tensors. The large grey arrow is the direction of Pacific – North America (PA/NA) motion. Composite stress tensors are shown along the bottom for focal mechanisms in the Graham Island region (left), Hecate Strait region (middle), and the combined Graham Island – Hecate Strait regions (right). The combined Graham Island – Hecate Strait stress tensor is likely representative of the stress field for the Queen Charlotte Islands region.

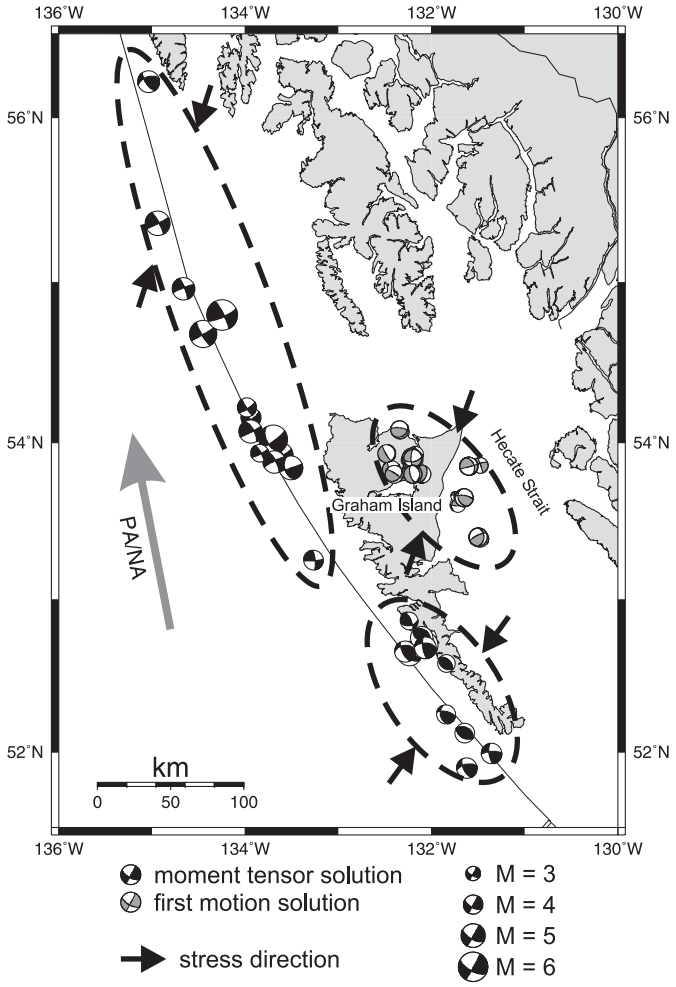

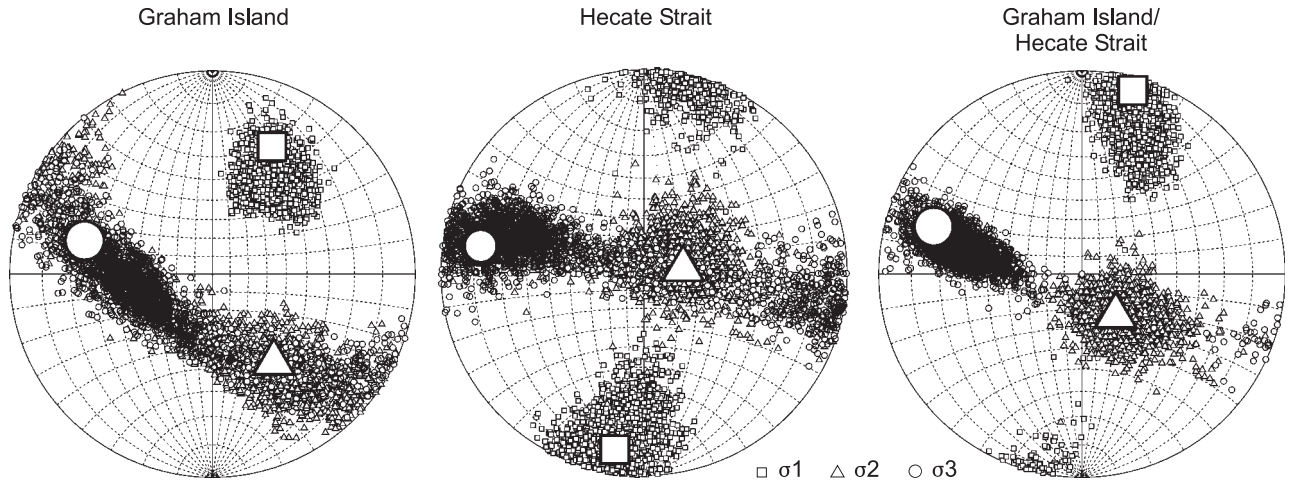

sible interpretation of the available focal mechanism and stress tensor data for the Queen Charlotte Islands region will be presented here.

The stress tensor for the Graham Island – Hecate Strait region is likely representative of the stress field for the Queen Charlotte Islands region, with σ1 having an azimuth of 20°. The maximum compressive stress is then oriented ~45° to the strike of the northern Queen Charlotte fault segment and

~60° to the strike of the southern Queen Charlotte fault segment. Unlike the northern segment of the Queen Charlotte fault, the southern segment had virtually no strike-slip RMT solutions associated with it during the study period. However, the 24 June 1970 M = 7 earthquake at the southern tip of the Queen Charlotte Islands had a mechanism that was mainly strike-slip with a significant northeast thrust component (Rogers 1986). This suggests that, over time, enough strain can be built up along the fault to initiate strike-slip faulting even with $\sigma 1$ oriented at high angles to the fault. However, the optimal orientation for $\sigma 1$ relative to the fault may be closer to 45° to initiate strike-slip faulting, which would suggest that the Queen Charlotte fault is a strong fault. Smith et al. (2003) measured heat flow values across the Queen Charlotte fault and did not find evidence for a heat flow anomaly associated with fault. This would imply a weak fault, similar to the San Andreas fault; however, large gradients in the measured heat flow values across the fault make it difficult to draw any firm conclusions about the lack of a Queen Charlotte fault heat flow anomaly. Therefore, the absence of a measured heat flow anomaly across the Queen Charlotte fault should not be taken as evidence of a weak fault.

Summary and conclusions

The overall regional stress pattern in western Canada mapped from moment tensor solutions and available first-motion focal mechanisms show mainly NE–SW *P* axis orientations. The exception is southern British Columbia where the compressive stress regime changes to north–south because of oblique subduction of the Juan de Fuca plate, right lateral shear motion of the Pacific and North America plates, and the rotation of the Washington and Oregon fore-arc blocks. The moment tensor solutions suggest that north–south compression may extend through southern British Columbia and northern Washington to the eastern Cordillera. However, this is a tectonically complex region with a transition from extensional to compressional tectonics, and it is not possible to determine the dominant tectonic force solely from the moment tensor solutions.

In the northern Canadian Cordillera, the stress pattern changes from $\sigma 1$ oriented nearly east–west in the Nahanni region to nearly north–south in the central and northern Mackenzie Mountains, to NE–SW in the Richardson Mountains. In the central and northern Mackenzie Mountains, the largest earthquakes may occur on faults that are mechanically weak, unlike the Richardson Mountains and Nahanni regions, which show no evidence of low-shear-strength faults. Stress tensor analysis in the Yakutat collision zone is consistent with a steady change in $\sigma 1$ from east–west in the east to north–south in the west. Stress tensors in the southern Canadian Cordillera show a sharp transition of $\sigma 1$ from north–south south of 51°N to NE–SW north of 51°N. RMT solutions in the vicinity of the Canada – United States border show east–west tension and north–south compression that could represent the transition from compressional to extensional tectonics. The RMT solutions may provide a better idea of which faults are optimally aligned for failure in the prevailing stress field. This will have important implications for seismic hazard related to large thrust earthquakes in southern British Columbia and southern Alberta.

RMT solutions in the Vancouver Island – Puget Sound region do not show any obvious pattern in faulting style that reflects the complex tectonic environment. The stress tensor results are poorly constrained but indicate margin-parallel compression in the crust and downdip tension in the subducting slab. The southern Queen Charlotte Islands region was dominated by high-angle thrust faults during the study period which provides evidence of Pacific – North America convergence, but cannot discriminate between underthrusting of the Pacific plate or deformation within the North America plate. Stress tensor analysis for the Queen Charlotte Islands region gives compressive stress directions that are consistent with average *P* axis directions from smaller earthquakes calculated by Bird (1997) for both the Queen Charlotte fault and the Graham Island – Hecate Strait region. The $\sigma 1$ value for the Queen Charlotte Islands region is oriented ~45° to the strike of the northern segment of the Queen Charlotte fault, where there is an abundance of strike-slip faulting, and ~60° to the strike of the southern segment of the fault, where virtually no strike-slip faulting was observed during the study period. This suggests that $\sigma 1$ may need to be oriented close to 45° to the strike of the fault to initiate strike-slip faulting, which would give it a higher shear strength than the San Andreas fault. However, the results do not conclusively show that strike-slip faulting cannot occur along the fault with $\sigma 1$ oriented at higher angles to the fault, as evidenced by the 24 June 1970 event at the southern end of the Queen Charlotte Islands.

The RMT solutions presented here provide valuable new insights into the contemporary stress regime in western Canada. Many of the solutions are in regions where very few focal mechanisms have previously been calculated and, as a consequence, little data related to stress was available. As the western Canada RMT database continues to grow, the results presented here can be refined and more information related to the state of stress in western Canada can be determined.

Acknowledgements

The authors would like to thank Chuck Ammon for providing the moment tensor code and for a great deal of valuable advice and suggestions on calculating regional moment tensor solutions. Stephane Mazzotti, Associate Editor Fred Cook, and two anonymous reviewers provided valuable comments that helped improve this manuscript. Many of the figures were created using Generic Mapping Tools (GMT) (Wessel and Smith 1991).

References

Adams, J. 1987. Canadian crustal stress database: a compilation to 1987. Geological Survey of Canada, Open File 1622.

Adams, J., and Bell, J.S. 1991. Crustal stresses in Canada. *In* Neotectonics of North America. *Edited by* D.B. Slemmons, E.R. Engdahl, M.D. Zoback, and D.D. Blackwell. Geological Society of America, Boulder, Colo., Decade Map, Vol. 1, pp. 367–386.

Ammon, C.J. 2001. Moment-tensor inversion overview [online]. Available from www.essc.psu.edu/~ammon/HTML/MTinvDocs/mtinv.html (cited 17 May 2005).

Angelier, J. 1979. Determination of the mean principal directions of stresses for a given fault population. Tectonophysics, **56**: T17–T26.

Angelier, J. 1984. Tectonic analysis of fault slip data sets. Journal of Geophysical Research, **89**: 5835–5848.

Atwater, T. 1989. Plate tectonic history of the northeast Pacific and western North America. *In* The Eastern Pacific Ocean and Hawaii. *Edited by* E.L. Winterer, D.M. Hussong, and R.W. Decker. Geological Society of America, Boulder, Colo., The Geology of North America, Vol. N, pp. 21–72.

Bérubé, J., Rogers, G.C., Ellis, R.M., and Hasselgren, E.O. 1989. A microseismicity study of the Queen Charlotte Islands region. Canadian Journal of Earth Sciences., **26**: 2556–2566.

Bird, A.L. 1997. Earthquakes in the Queen Charlotte Islands region: 1982–1996. M.Sc. thesis, School of Earth and Ocean Sciences, University of Victoria, Victoria, B.C.

Bolton, M.K. 2003. Juan de Fuca plate seismicity at the northern end of the Cascadia subduction zone. M.Sc. thesis, School of Earth and Ocean Sciences, University of Victoria, Victoria, B.C.

Braunmiller, J. 1998. Seismotectonics of the Explorer region and Blanco transform fault zone. Ph.D. dissertation, College of Oceanic and Atmospheric Sciences, Oregon State University, Corvallis, Ore.

Braunmiller, J., and Nábělek, J. 2002. Seismotectonics of the Explorer region. Journal Geophysical Research, **107**(B10): 2208.

Brune, J.N., Henyey, T.L., and Roy, R.F. 1969. Heat flow, stress, and rate of slip along the San Andreas fault, California. Journal of Geophysical Research, **74**: 3821–3827.

Cassidy, J.F., and Bent, A.L. 1993. Source parameters of the 29 May and 5 June 1940 Richardson Mountains earthquakes. Bulletin of the Seismological Society of America, **83**: 636–659.

Cassidy, J.F., Schmitt, S., and Bent, A.L. 2002. The 1953–1957 Mackenzie Mountains earthquake sequence. Seismological Research Letters, **73**: 221A.

Cassidy, J.F., Rogers, G.C., and Ristau, J. 2005. Seismicity in the vicinity of the SNORCLE corridors of the northern Canadian Cordillera. Canadian Journal of Earth Sciences, **42**: 1137–1148.

Doser, D.I., and Lomas, R. 2000. The transition from strike-slip to oblique subduction in southeastern Alaska from seismological studies. Tectonophysics, **316**: 45–65.

Dragert, H., Hyndman, R.D., Rogers, G.C., and Wang, K. 1994. Current deformation and the width of the seismogenic zone of the northern Cascadia subduction thrust. Journal of Geophysical Research, **99**: 653–668.

Dziewonski, A.M., Chou, T.-A., and Woodhouse, J.H. 1981. Determination of earthquake source parameters from waveform data for studies of global and regional seismicity. Journal of Geophysical Research, **86**: 2825–2852.

Estabrook, C.H., Nábělek, J.L., and Lerner-Lam, A.L. 1992. Tectonic model of the Pacific-North America plate boundary in the Gulf of Alaska from broadband analysis of the 1979 St. Elias, Alaska, earthquake and its aftershocks. Journal of Geophysical Research, **97**: 6587–6612.

Fletcher, H.J., and Freymueller, J.T. 1999. New GPS constraints on the motion of the Yakutat Block. Geophysical Research Letters, **26**: 3029–3032.

Frolich, C., and Davis, S.D. 1999. How well constrained are well-constrained *T*, *B*, and *P* axes in moment tensor catalogues?. Journal of Geophysical Research, **104**: 4901–4910.

Gephart, J.W., and Forsyth, D.W. 1984. An improved method for determining the regional stress tensor using earthquake focal mechanism data: application to the San Fernando earthquake sequence. Journal of Geophysical Research, **89**: 9305–9320.

Glombick, P., Thompson, R.I., Erdmer, P., and Daughtry, K.L. 2006. A reappraisal of the tectonic significance of early Tertiary low-angle shear zones exposed in the Vernon map area (82L), Shuswap metamorphic complex, southeast Canadian Cordillera. Canadian Journal of Earth Science. **43**: 245–268.

Hardebeck, J.L., and Hauksson, E. 2001. Crustal stress field in southern California and its implications for fault mechanics. Journal of Geophysical Research, **106**: 21 859 – 21 882.

Hardebeck, J.L., and Michael, A.J. 2004. Stress orientations at intermediate angles to the San Andreas fault, California. Seismological Research Letters, **75**: 244A. [Abstract:]

Hildebrand, R.S., Hoffman, P.F., and Bowring, S.A. 1987. Tectonic magmatic evolution of the 1.9-Ga Great Bear Magmatic Zone, Wopmay orogen, NW Canada. Journal of Volcanology and Geothermal Research, **32**: 39–50.

Hoffman, P.F., and Bowring, S.A. 1984. Short-lived 1.9-Ga continental margin and its destruction, Wopmay orogen. Geology, **12**: 68–72.

Hyndman, R.D., and Ellis, R.M. 1981. Queen Charlotte fault zone: microearthquakes from a temporary array of land stations and ocean bottom seismographs. Canadian Journal of Earth Sciences, **18**: 776–788.

Hyndman, R.D., and Hamilton, T.S. 1993. Queen Charlotte area Cenozoic tectonics and volcanism and their association with relative plate motion along the northeastern Pacific margin. Journal of Geophysical Research, **98**: 14 257 – 14 277.

Hyndman, R.D., and Wang, K. 1995. The rupture zone of Cascadia great earthquakes from current deformation and the thermal regime. Journal of Geophysical Research, **100**: 22 133 – 22 154.

Hyndman, R.D., Flück, P., Mazzotti, S., Lewis, T., Ristau, J., and Leonard, L. 2005. Current tectonics of the northern Canadian Cordillera. Canadian Journal of Earth Sciences, **42**: 1117–1136.

Isachsen, C.E., and Bowring, S.A. 1994. Evolution of the Slave craton. Geology, **22**: 917–920.

Jones, L.M. 1988. Focal mechanisms and the state of stress on the San Andreas fault in southern California. Journal of Geophysical Research, **93**: 8869–8891.

Lachenbruch, A.H., and Sass, J.H. 1992. Heat flow from Cajon Pass, fault strength, and tectonic implications. Journal of Geophysical Research, **97**: 4995–5015.

Lahr, J.C., and Plafker, G. 1980. Holocene Pacific – North America plate interaction in southern Alaska: implications for the Yakataga seismic gap. Geology, **8**: 483–486.

Lahr, J.C., Plafker, G., Stephens, C.O., Fogleman, K.A., and Blackford, M.E. 1979. Interm report on the St. Elias earthquake of 28 February 1979. US. Geological Survey, Open File Report 79-670.

Langston, C.A. 1981. Source inversion of seismic waveforms: the Koyna, India, earthquakes of 13 September, 1967. Bulletin of the Seismological Society of America, **71**: 1–24.

Mazzotti, S., and Hyndman, R.D. 2002. Yakutat collision and strain transfer across the northern Canadian Cordillera. Geology, **30**: 495–498.

Mazzotti, S., Dragert, H., Henton, J., Schmidt, M., Hyndman, R., James, T., Lu, Y., and Craymer, M. 2003*a*. Current tectonics of northern Cascadia from a decade of GPS measurements. Journal of Geophysical Research, **108**: 2554.

Mazzotti, S., Hyndman, R.D., Flück, P., Smith, A.J., and Schmidt, M. 2003*b*. Distribution of the Pacific/North America motion in the Queen Charlotte Islands-S. Alaska plate boundary zone. Geophysical Research Letters, **30**: 1762.

McKenzie, D.P. 1969. The relation between fault plane solutions for earthquakes and the directions of principal stresses. Bulletin of the Seismological Society of America, **59**: 591–601.

Menard, H. 1978. Fragmentation of the Farallon plate by pivoting subduction. Journal of Geophysical Research, **86**: 99–110.

Michael, A.J. 1984. Determination of stress from slip data: faults and folds. Journal of Geophysical Research, **89**: 11 517 – 11 526.

Michael, A.J. 1987. Use of focal mechanisms to determine stress: a control study. Journal of Geophysical Research, **92**: 357–368.

Monger, J.W.H., and Price, R.A. 1979. Geodynamic evolution of the Canadian Cordillera — progress and problems. Canadian Journal of Earth Sciences, **16**: 770–791.

Mulder, T.L. 1995. Small earthquakes in southwest British Columbia (1975–1991). M.Sc. thesis, School of Earth and Ocean Sciences, University of Victoria, Victoria, B.C.

Parrish, R.R., Carr, S.D., and Parkinson, D.L. 1988. Eocene extensional tectonics and geochronology of the southern Omineca belt, British Columbia and Washington. Tectonics, **7**: 181–212.

Plafker, G., Moore, J.C., and Winkler, G.R. 1994. Geology of the southern Alaska margin. *In* The geology of Alaska. *Edited by* G. Plafker and H.C. Berg Geological Society of America, Boulder, Colo., The geology of North America, Vol. G1, pp. 389–451.

Provost, A-S., and Houston, H. 2001. Orientation of the stress field surrounding the creeping section of the San Andreas fault: evidence for a narrow mechanically weak fault zone. Journal of Geophysical Research, **106**: 11 373 – 11 386.

Provost, A.-S., and Houston, H. 2003. Stress orientations in northern and central California: evidence for the evolution of frictional strength along the San Andreas plate boundary system. Journal of Geophysical Research, **108**: 2175.

Ratchkovski, N.A., Hansen, R.A., Stachnik, J.C., Cox, T., Fox, O., Rao, L., Clark, E., Lafevers, M., Estes, S., MacCormack, J.B., and Williams, T. 2003. Aftershock sequence of the M_w 7.9 Denali fault, Alaska earthquake of 3 November 2002 from regional seismic network data. Seismological Research Letters, **74**: 743–752.

Riddihough, R.P. 1977. A model for recent plate interactions off Canada's west coast. Canadian Journal of Earth Sciences, **14**: 384–396.

Riddihough, R.P. 1984. Recent movements of the Juan de Fuca plate system. Journal of Geophysical Research, **89**: 6980–6994.

Riddihough, R.P., and Hyndman, R.D. 1989. Queen Charlotte Islands margin. *In* The Eastern Pacific Ocean and Hawaii. *Edited by* E.L. Winterer, D.M. Hussong, and R.W. Decker. The Geological Society of America, Boulder, Colo., The geology of North America, Vol. N, pp. 403–411.

Ristau, J.P. 2004. Seismotectonics of western Canada from regional moment tensor analysis. Ph.D. dissertation, School of Earth and Ocean Sciences, University of Victoria, Victoria, B.C.

Ristau, J., Rogers, G.C., and Cassidy, J.F. 2003. Moment magnitude–local magnitude calibration for earthquakes off Canada's west coast. Bulletin of the Seismological Society of America, **93**: 2296–2300.

Ristau, J., Rogers, G.C., and Cassidy, J.F. 2005. Moment magnitude–local magnitude calibration for earthquakes in western Canada. Bulletin of the Seismological Society of America, **95**: 1994–2000.

Rogers, G.C. 1986. Seismic gaps along the Queen Charlotte fault. Earthquake Prediction Research, **4**: 1–11.

Rogers, G.C. 1998. Earthquakes and earthquake hazard in the Vancouver area. *In* Geology and natural hazards of the Fraser River Delta, British Columbia. *Edited by* J.J. Clague, J.L. Luternauer, and D.C. Mosher. Geological Survey of Canada, Bulletin 525, pp. 17–25.

Rogers, G.C., Ellis, R.M., and Hasegawa, H.S. 1980. The McNaughton Lake earthquake of May 14, 1978. Bulletin of the Seismological Society of America, **70**: 1771–1786.

Rohr, K.M.M., Scheidhauer, M., and Trehu, A.M. 2000. Transpression between two warm mafic plates: The Queen Charlotte Fault revisited. Journal of Geophysical Research, **105**: 8147–8172.

Saffer, D.M., Bekins, B.A., and Hickman, S. 2003. Topographically driven groundwater flow and the San Andreas heat flow paradox revisited. Journal of Geophysical Research, **108**: 2274.

Sbar, M.L., Barazangi, M., Dorman, J., Scholz, C.H., and Smith, R.B. 1972. Tectonics of the Intermountain Seismic Belt, western United States: microearthquake seismicity and composite fault plane solutions. Geological Society of America Bulletin, **83**: 13–28.

Sipkin, S.A. 1986. Estimation of earthquake source parameters by the inversion of waveform data: global seismicity. Bulletin of the Seismological Society of America, **76**: 1515–1541.

Smith, A.J., Hyndman, R.D., Cassidy, J.F., and Wang, K. 2003. Structure, seismicity and thermal regime of the Queen Charlotte transform margin. Journal of Geophysical Research, **108**(B11): 2539.

Stickney, M.C., and Bartholomew, M.J. 1987. Seismicity and late Quaternary faulting of the northern Basin and Range Province, Montana and Idaho. Bulletin of the Seismological Society of America, **77**: 1602–1625.

Stickney, M.C., and Lageson, D.R. 2002. Seismotectonics of the 20 August 1999 Red Rock Valley, Montana, earthquake. Bulletin of the Seismological Society of America, **92**: 2449–2464.

Townend, J., and Zoback, M.D. 2001. Implications of earthquake focal mechanisms for the frictional strength of the San Andreas fault system. *In* The nature and tectonic significance of fault zone weakening. *Edited by* R.E. Holdsworth, R.A. Strachan, J.F. Magloughlin, and R.J. Knipe. Geological Society (of London), Special Publication 186, pp. 13–21.

Townend, J., and Zoback, M.D. 2004. Regional tectonic stress near the San Andreas fault in central and southern California. Geophysical Research Letters, **31:** L15S11. doi:10.1029/2003GL018918.

Wang, K., He, J., and Davis, E.E. 1997. Transform push, oblique subduction resistance, and intraplate stress of the Juan de Fuca plate. Journal of Geophysical Research, **102**: 661–674.

Wells, R.E., Weaver, C.S., and Blakely, R.J. 1998. Fore-arc migration in Cascadia and its neotectonic significance. Geology, **206**: 759–762.

Wessel, P., and Smith, W.H.F. 1991. Free software helps map and display data. EOS, **72**: 441.

Wetmiller, R.J., Horner, R.B., Hasegawa, H.S., North, R.G., Lamontagne, M., Weichert, D.H., and Evans, S.G. 1988. An analysis of the 1985 Nahanni earthquakes. Bulletin of the Seismological Society of America, **78**: 590–616.

Wiemer, S. 2001. A software package to analyse seismicity, ZMAP. Seismological Research Letters, **72**: 373–382.

Wilson, D.S. 1988. Tectonic history of the Juan de Fuca ridge over the last 40 million years. Journal of Geophysical Research, **93**: 11863–11876.

Zoback, M.L., and Zoback, M. 1980. State of stress in the Conterminous United States. Journal of Geophysical Research, **85**: 6113–6156.